A&A 464, 715–734 (2007)
DOI: 10.1051/0004-6361:20066175

Astronomy & Astrophysics

The He II Fowler lines and the O III and N III Bowen fluorescence lines in the symbiotic nova RR Telescopii

P. Selvelli[1], J. Danziger[1], and P. Bonifacio[2,3,1]

[1] INAF – Osservatorio Astronomico di Trieste, via Tiepolo 11, 34143 Trieste, Italy
e-mail: selvelli@ts.astro.it
[2] CIFIST Marie Curie Excellence Team
[3] Observatoire de Paris, GEPI, 5 place Jules Janssen, 92195 Meudon, France

Received 3 August 2006 / Accepted 17 December 2006

ABSTRACT

Aims. A detailed study of the O III and N III Bowen lines in the spectrum of RR Tel.
Methods. Absolute intensities for the He II, O III, and N III emission lines have been obtained from STIS, UVES, FEROS and IUE data, after re-calibration of UVES and FEROS on the STIS scale.
Results. A new measure of reddening ($E_{(B-V)} \sim 0.00$) has been obtained from the comparison between the observed and the theoretical intensity decrement for 20 emission lines of the He II Fowler ($n \rightarrow 3$) series. This value has been confirmed by the STIS and IUE continuum distribution, and by the value of $n_{\rm H}$ from the damped profile of the IS H Ly-α line. We have obtained very accurate measurements for about thirty Bowen lines of O III and a precise determination of the efficiency in the O1 and O3 excitation channels (18% and 0.7%, respectively). The relative O III intensities are in good agreement with the predictions by Froese Fischer (1994). A detailed study of the decays from all levels involved in the Bowen mechanism has lead to the detection of two new O III Bowen lines near λ 2190. High resolution IUE data have shown a nearly linear decline with time, from 1978 to 1995, in the efficiency of the O1 and O3 processes, with a steeper slope for the O3 channel. A detailed study of the N III λ 4640 lines and of their excitation mechanism has shown that, recombination and continuum fluorescence being ruled out, line fluorescence remains the only viable mechanism to pump the 3d $^2D_{5/2}$ and 3d $^2D_{3/2}$ levels of N III. We point out the important role of multiple scattering in the resonance lines of O III and N III near λ 374 and show that the observed N III line ratios and intensities can be explained in terms of line fluorescence by the three resonance lines of O III at $\lambda\lambda$ 374.432, 374.162 and 374.073 under optically thick conditions.

Key words. stars: novae, cataclysmic variables – stars: binaries: symbiotic – ultraviolet: stars – atomic processes – radiative transfer

1. Introduction

RR Tel is one of the slowest of all novae and is still evolving in the nebular stage more than 60 years after the outburst of Oct. 1944. RR Tel has been classified also as a symbiotic nova on account of the presence of an M5 III star in the binary system. In 1949 the nova remnant started to shrink back to white dwarf dimensions: the visual brightness began a gradual decline, although the stellar temperature increased, and the nebular emission showed a slow evolution toward an increasing degree of ionization (Mayall 1949; Thackeray 1977; Murset & Nussbaumer 1993). A distinctive peculiarity of RR Tel is the richness and complexity of its emission spectrum that spans a wide range of ionization and excitation. The simultaneous presence of spectral features attributable to: 1) the hot nova remnant with $T_{\rm eff}$ about 150 000 K (Hayes & Nussbaumer 1986, hereinafter HN86), 2) the M5 III companion star with semi-regular Mira-like pulsations ($P \sim 387^{\rm d}$) (Henize & McLaughlin 1951; Feast et al. 1977), 3) a slowly expanding nebula illuminated by the hot remnant, 4) the "shocked" region where, allegedly, the wind from the giant and the wind of the nova interact (Contini & Formiggini 1999), 5) an IR excess whose origin is quite uncertain (free-free, dust), makes RR Tel an ideal laboratory for studies of low-density astrophysical plasmas.

The recent availability of very good quality UVES and STIS data of RR Tel has prompted us to combine them together, with the purpose of fully exploiting the best characteristics of these two instruments, i.e. the high spectral resolution of STIS in the UV and UVES in the optical, together with the wide wavelength coverage with absolutely calibrated data by STIS. This has allowed the detection of weak spectral features and accurate measurement of absolute emission line intensities (ELI) and line ratios. Data from FEROS (with resolution comparable to that of UVES) have been also used to complement the STIS data for N III in the two spectral regions near λ 4100 and λ 4640, not covered by UVES. High resolution IUE data in the LW region have also been used to follow the changes in the He II and O III line intensities from 1978 to 1995.

2. The spectroscopic data

2.1. HST-STIS data

We have retrieved from the HST archive the STIS spectra secured on Oct. 10, 2000 as part of program 8098 (see Keenan et al. 2002). The instrument setup included the echelle gratings E140M and E230M with FUV and NUV MAMA detectors, and the first-order gratings G430M and G750M with CCD detectors. The datasets are listed in Table 1, together with some relevant spectroscopic information. We note that the E140 M and E230 M echelle gratings together cover the spectral range from 1150 to 3110 Å, while the data obtained with the G430M and G750M first-order gratings cover the range from 3025 to 7100 Å. The absolute fluxes are accurate within 8%

Table 1. The STIS dataset.

Dataset	Filter-gra	Resolution	Detector	Aperture
O5EH01010	E140M	45 800	FUV-MAMA	0.2×0.2
O5EH01020	G430M	5330–10 270	CCD	52×0.2
O5EH01030	E230M	30 000	NUV-MAMA	0.2×0.2
O5EH01040	G430M	5330–10 270	CCD	52×0.2
O5EH01050	G430M	5330–10 270	CCD	52×0.2
O5EH01060	G430M	5330–10 270	CCD	52×0.2
O5EH01070	G430M	5330–10 270	CCD	52×0.2
O5EH01080	G430M	5330–10 270	CCD	52×0.2
O5EH01090	E230M	30 000	NUV-MAMA	0.2×0.2
O5EH010A0	G430M	5330–10 270	CCD	52×0.2
O5EH010B0	G430M	5330–10 270	CCD	52×0.2
O5EH010C0	G430M	5330–10 270	CCD	52×0.2
O5EH010D0	G430M	5330–10 270	CCD	52×0.2
O5EH010E0	G750M	4870–9950	CCD	52×0.2
O5EH010F0	G750M	4870–9950	CCD	52×0.2
O5EH010G0	G750M	4870–9950	CCD	52×0.2

(MAMA) and 5% (CCD), while the wavelengths are accurate to 1.5–5.0 km s^{-1} (MAMA) and 3–15 km s^{-1} (CCD) (we refer to the `www.stsci.edu/hst/stis/performance/accuracy/document.html` page for more detailed information).

The STIS data have been recently (Dec. 2003) re-calibrated to allow for the effects of increasing CCD charge transfer inefficiency (due to the accumulated effects of radiation exposure) and for the effects of time-dependent optical sensitivity. The work in the present paper is based on these recent data.

2.2. UVES data

For a description of the UVES spectra (obtained on Oct. 16th, 1999) and their reduction we refer to Selvelli & Bonifacio (2000). We note that the spectral resolution on UVES is close to 55 000, for the red arm spectra, taken with a 0.″8 slit and slightly higher (~65 000) for the blue arm spectra, where the slit was 0.″6. The seeing conditions during UVES observations (mid Oct. 1999) were around 0.72–0.75 arcsec. The angular size of the RR Tel nebula is less than 0.1 arcsec, since its radius is near to 1.0×10^{15} cm (HN86) and the distance is about 3500 pc (see Sect. 3.5).

No spectrophotometric standard star was observed that night, so the data presented in Selvelli & Bonifacio (2000) were simply normalized to the continuum. The instrument response function may be, nevertheless, estimated by using observations of a spectrophotometric standard star taken on a different night. For this we used the observations of the white dwarf EGGR 21 (Stone & Baldwin 1983; Bessel 1999) taken on September 26th 1999, observed with the same spectrograph setting as RR Tel but with a slit width of 10″. The UVES spectrum thus calibrated is not suitable for flux measurements due to: a) the unknown slit losses, when observing with a narrow slit (smaller than the seeing *FWHM*); b) possible differences in atmospheric extinctions between the night in which RR Tel was observed and the night in which EGGR 21 was observed. We therefore decided to make use of the flux calibrated STIS spectrum to re-calibrate the UVES spectrum, in the ranges $\lambda\lambda$3040–3820 and $\lambda\lambda$ 5500–5700. We did so by forcing the continuum of the UVES spectrum to coincide with that of the STIS absolute distribution after proper f_λ correction in selected line-free windows.

This has allowed us to obtain reliable emission line intensities (ELI) and reliable line ratios also for some (weak) O III emission lines that are clearly observed in UVES spectra but are not detected or are confused with noise in the STIS grating spectra in the optical range.

This procedure could be criticized since the STIS data have been secured about 1 year after the UVES ones, and the star flux is not constant with time. However, it is justified by the fact that the variations in the continuum and ELI of RR Tel are supposed to be quite slow with a time-scale of years (Murset & Nussbaumer 1993; Zuccolo et al. 1997). It is also justified, "a posteriori", by the fact that the ELI measured in STIS and UVES spectra (after this recalibration) give a nearly constant (~1.16 ± 0.03) ratio for those O III lines that are common to the two groups of spectra. See also Sect. 4.5 for a descripion of the absolute ELI changes in the last twenty years for He II and O III.

From the STIS/UVES ELI ratios nothing can be said about any absolute ELI changes between Oct. 1999 (UVES) and Oct. 2000 (STIS). One can only guess that most ELI have followed the general trend of a slow decline, following the continuum, with the possible exception of the high excitation and/or high ionization lines whose ELI could have increased.

2.3. IUE data

The IUE spectra have been retrieved from the INES (IUE Newly Extracted Spectra) final archive. For a detailed description of the IUE-INES system see Rodriguez-Pascual et al. (1999) and Gonzalez-Riestra et al. (2001).

For a new determination of the UV continuum (see Sect. 3.2) we have used all available low resolution IUE spectra taken with the large aperture, with the exception of the very few spectra (e.g. SWP05836, SWP05885, SWP13730, SWP4603) that have shown saturation in the continuum or other problems in the exposure.

High resolution IUE-INES data have been used in Sect. 4.5 for measuring the intensity in 1978–1995 of some He II Fowler lines (λ 2733 and λ 3203) and some O III Bowen lines ($\lambda\lambda$ 2836, 3047, 3122, and 3133). The LWP and LWR spectra are those reported in Table 6, and have been individually checked for their quality. They are not or only mildly affected by saturation effects or by camera artifacts. A few IUE spectra that were over/under exposed or affected by factors such as bad guiding, high background noise, microphonic noise, etc. have been disregarded. The quality flags for the λ 3133 line generally indicate the presence of a fiducial mark near the spectrum, but this reseau is located outside of it. The quality flags indicates also the marginal presence of a few saturated pixels in the spectra with longer exposure time.

2.4. FEROS data

We made use of the FEROS commissioning data (Kaufer et al. 1999) which are available through the FEROS Spectroscopic Database at the LSW Heidelberg (`http://www.lsw.uni-heidelberg.de/projects/instrumentation/Feros/ferosDB`) to measure the N III lines near λ 4640 and λ 4100 (see Sect. 6.2), which are not covered by the spectra of the other instruments. These 4 spectra were acquired on October 7th 1998, one has an exposure time of 300 s, the other three of 600 s. The standard extracted, flat-fielded, wavelength calibrated, and merged spectrum of both object and sky fibres have been downloaded from the database. The spectra cover the range 3520–9210 Å with a resolution $R \sim 60\,000$. Also for FEROS, in a similar way as that for UVES, we have made use of the flux calibrated STIS spectra to re-calibrate the

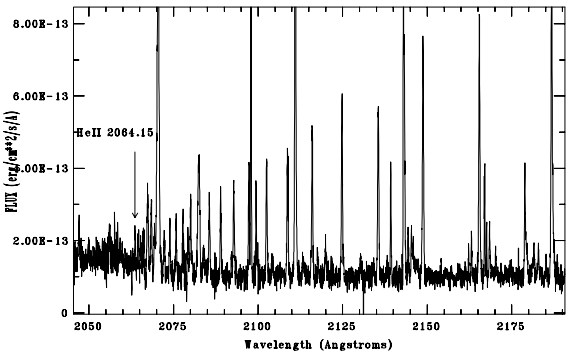

Fig. 1. The He II Fowler lines near the head of the $(n - 3)$ series. The last resolved line is (37-3) λ 2063.49.

FEROS spectrum, in the range $\lambda\lambda$ 4100–4700. We did so by forcing the continuum of FEROS to coincide with that of STIS in selected line-free windows. This has allowed us to measure reliable ELI and reliable line ratios for a few N III emission lines that are clearly observed in FEROS spectra but are not detected or are confused with noise in the STIS grating spectra. The same warnings and considerations given in Sect. 2.2 are valid here. However, also in this case, the procedure is justified by the fact that the ELI measured in STIS and (re-calibrated) FEROS spectra give a nearly constant (∼1.18 ± 0.02) ratio for the N III lines that are in common to the two spectra.

3. The reddening and the distance

3.1. The He II recombination lines

We have adopted and updated the method of Penston et al. (1983) of comparing the observed intensities of the He II ($n \rightarrow 3$) recombination lines with the corresponding theoretical ratios in order to obtain an estimate of the color excess E_{B-V}. Incidentally we point out, that these ($n \rightarrow 3$) transitions are often named as "Paschen" lines in the astronomical literature, irrespective of their belonging to HI or He II, while the He II ($n \rightarrow 3$) lines should be correctly named as "Fowler" lines (as in Table 4.3 of Osterbrock & Ferland 2006) and hereinafter they will be named so.

The STIS data provide an optimum coverage for the whole set of the He II Fowler lines, from λ 4685.71 down to the region of the head of the series near λ 2063 (Fig. 1).

The spectral region between $\lambda\lambda$ 2025 and 2300 is quite interesting because it has remained "unexplored" until recent times: all of the IUE spectra suffered from severe underexposure in this range because of the extremely low response of the LW cameras below λ 2300, and the HST-GHRS data cover only a short range in some selected spectral regions. In the STIS spectra, the very good spectral resolution allows one to resolve the lines up to the (37 → 3) transition at λ 2063.49, very near to the series limit (Fig. 1). We recall that in the UVES spectra the hydrogen Balmer lines were instead resolved up to the (38 → 2) transition (Selvelli & Bonifacio 2000).

In a study of RR Tel from IUE data, HN86 from various diagnostic methods based on ratios of collisionally excited lines, have derived log $N_e \sim 6.0$ and $T_e \sim 12\,500$ K. Adopting these values (we note, however, that the relative lines strengths in the recombination spectrum of He II have little dependence on electron temperature and density) we have compared our observed relative strengths of the various He II Fowler lines (normalized to $I_{4686} = 100$) with the theoretically derived ratios for "case B" by Storey & Hummer (1995). The "case B" assumption is justified by the presence itself of strong O III Bowen lines (that require large optical depth in the He II Ly-α line, see in the following) and by the observed I_{3203}/I_{4686} ratio ∼0.43, that is generally associated with "case B" (see Schachter et al. 1991).

Table 2. He II Fowler Emission Lines. The air wavelength (Å), the ELI (10^{-13} erg cm^{-2} s^{-1}) and the *FWHM* (km s^{-1}) of the He II emission lines in STIS. The theoretical values I_{th} (Storey & Hummer 1995) correspond to log N_e = 6.0 and T_e = 12 500 K.

λ_{air}	ELI	*FWHM*	I_{obs}/I_{4686}	I_{th}/I_{4686}	ratio
4685.71	147.50	56.2	100.0	100.0	1.00
3203.10	63.52	54.2	43.0	43.7	0.99
2733.30	32.33	56.1	21.9	23.1	0.95
2511.20	18.98	56.4	12.9	13.9	0.93
2385.40	12.60	57.3	8.54	9.03	0.95
2306.19	9.23	56.2	6.26	6.25	1.00
2252.69	6.25	56.1	4.24	4.52	0.94
2186.60	3.96	63.5	2.68	2.60	1.03
2165.25	2.81	51.4	1.91	2.01	0.95
2148.60	2.60	55.1	1.76	1.68	1.05
2133.35	1.98	55.1	1.34	1.40	0.96
2124.63	1.80	50.8	1.22	1.18	1.03
2115.82	1.51	48.2	1.02	1.02	1.00
2108.50	1.34	56.2	0.91	0.90	1.01
2102.35	1.17	52.8	0.79	0.79	1.00
2097.12	1.00	54.8	0.68	0.71	0.96
2092.64	.94	55.9	0.64	0.64	1.00
2088.72	.85	50.3	0.58	0.59	0.98
2085.41	.80	52.5	0.54	0.55	0.98
2079.88	.70	53.6	0.475	0.47	1.01
1640.42	831.10	63.2	563.4	702.1	0.81

Table 2 gives the observed He II ELI (10^{-13} erg cm^{-2} s^{-1}) for all transition of the Fowler series starting from λ 4686 (4 → 3) up to 2079.88 (25 → 3), with the exception of the λ 2214.67 (11 → 3) and λ 2082.47 (24 → 3) lines that are blended. Table 2 gives also the Gaussian *FWHM* in km s^{-1} (deconvolved from the instrumental *FWHM*), the observed and theoretical (for case B log N_e = 6.0 and T_e = 12 500 K) intensities relative to I_{4686} = 100, and, in the last column, the ratio I_{obs}/I_{4686} over I_{th}/I_{4686}. In the last line of Table 2 the corresponding values for the He II Ba-α line at λ 1640 are also given. The average *FWHM* for 20 unblended lines of the Fowler series is =53.5 ± 3.5 km s^{-1}. In Fig. 2 the I_{obs}/I_{th} ratio of Table 2 is plotted versus wavelength. The mean value of the points is 0.986, the median is 0.995, with standard deviation =0.033. The points clearly define a straight line with slope very near 0.00, thus clearly indicating that $E_{(B-V)} \sim 0.00$.

We recall that Penston et al. obtained $E_{(B-V)} = 0.10$, but their measurements were based on just a few He II lines and in spectra that were very noisy below λ 2400.

In this context, it should be pointed out that under the nebular conditions as in the RR Tel nebula, the large optical depth in the He II Ly-α line and its complex line transfer that is associated with the Bowen fluorescence (see Sect. 4) should not influence the He II Fowler lines, but could possibly affect the intensity of the He II Ba-α (3–2) line at λ 1640. In fact, the low I_{1640} over I_{4686} observed ratio =∼5.63 (instead of the theoretical one, close to 7.0, for log N_e = 6.0 and T_e = 12 500) is an indication that the line has developed some optical depth as a consequence of the "trapping" of the He II Ly-α line λ 304 that causes level 2 to be overpopulated. Also the larger width of the λ 1640 line (63 km s^{-1} as compared to the 55 km s^{-1} as the average value for the remaining He II lines) is indicative of its larger optical depth.

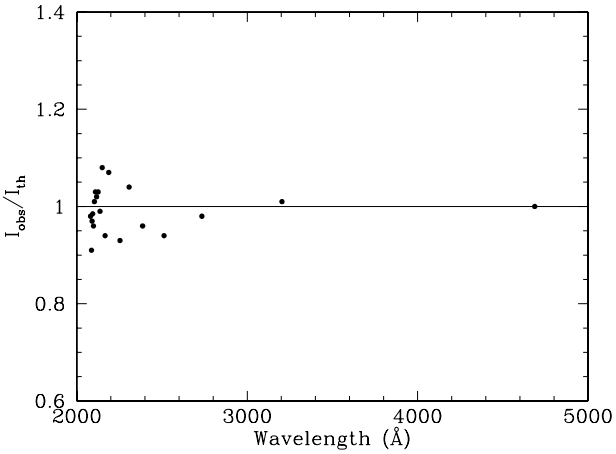

Fig. 2. The I_{obs}/I_{th} ratio relative to I_{4686} for the He II Fowler lines listed in Table 2.

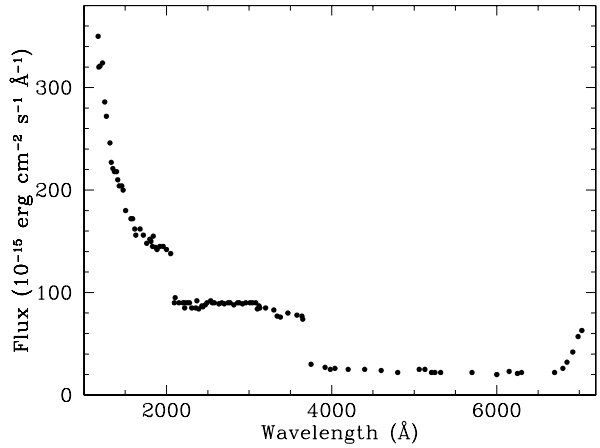

Fig. 3. The observed continuum of RR Tel, determined from line-free regions in the STIS spectrum. The b-f discontinuities of He II (Fowler series) and HI (Balmer series) are clearly evident. The rise of the continuum longward of λ 6800 is due to the contribution from the M giant companion star.

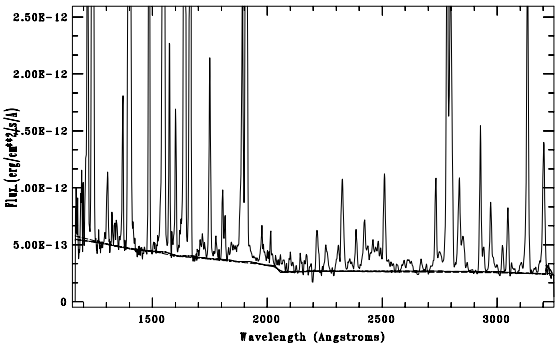

Fig. 4. The UV continuum in the average spectrum obtained by averaging and merging 39 SWP and 35 LW low resolution IUE spectra.

We note that the low I_{1640} over I_{4686} observed ratio comes from the low intensity of the λ 1640 line and not by an excessive intensity of the λ 4686 line since the decrements of all of the Fowler lines relative to I_{4686} are very close to the expected values (e.g. the I_{3203}/I_{4686} observed ratio is ∼0.43, to be compared to the theoretical ratio ∼0.44). It should be also mentioned that Netzer et al. (1985) in a study of Bowen fluorescence and He II lines in active galaxies and gaseous nebulae have considered the possibility of an increase in the population of $n = 4$ of He II through hydrogen Ly-α pumping from $n = 2$ to $n = 4$ of He II. This would result in an enhanced I_{4686} ($4 \rightarrow 3$) over I_{1640} ($3 \rightarrow 2$) ratio. However, this mechanism is not effective in RR Tel since, as mentioned, the intensity of the various Fowler lines relative to I_{4686} is very close to the expected one.

3.2. The STIS UV + optical continuua

Penston et al. (1983) confirmed the $E_{(B-V)} = 0.10$ value obtained from the He II lines with the presence (although rather weak) of the common interstellar absorption bump near λ 2200 in the continuum of IUE low resolution spectra.

In order to check for the alleged presence of this absorption bump we have exploited the high spectral resolution of STIS in the UV region and plotted the STIS continuum intensity versus wavelength in line-free regions. Figure 3 is self explanatory: the very flat near UV continuum distribution, and the intensity increase towards the far UV, is not consistent with what is generally observed in reddened objects. In Fig. 3 one can easily note the presence of the two bound-free discontinuities of He II and HI near λ 2060 and λ 3646 respectively with D(He II-Fowl) = log $I_{2060+}/I_{2060-} \sim 0.21$ and D(HI-Ba) = log $I_{3646+}/I_{3646-} \sim 0.48$.

In order to elucidate further the origin of the alleged IUE bump reported by Penston et al. (1983), we have coadded and merged all the IUE low resolution spectra available from the IUE VILSPA archive (large aperture only, not overexposed in the continuum) and created an "average" spectrum out of 39 SW and 35 LW spectra (Fig. 4). As result of the good S/N ratio also in the region below λ 2300, an inspection of the "average" spectrum definitely shows that there is no evidence of the IS absorption bump centered near lambda 2175. The absorption dip reported by Penston et al. (1983) comes probably from the "lack" of strong emission features in the region near λ 2200 (that could have have had the effect of "raising" the continuum in low resolution IUE spectra), and from the presence of the Fowler discontinuity. Also in the emission-line-free region near λ 2600 the effect is to mimic the presence of a similar (wide) absorption feature.

A comparison between the IUE continuum and the STIS continuum also confirms the near grey decline with time of the UV continuum.

3.3. The N_H column density towards RR Tel

From the profile of the damping wings of the IS Ly-α absorption line (Fig. 5) one can obtain the column density of neutral hydrogen towards RR Tel. Only the blue wing can be used, since the red wing is affected by the rather strong O V] emission line λ 1218.34. The blue wing itself is partially contaminated by the [O V] λ 1213.81 emission line. This adds further uncertainity to the derived column density. Our best-fit value, obtained by excluding the interval contaminated by O V] λ 1213.80, is $N_H \sim 6.9 \times 10^{19}$ (atoms cm^{-2}) with a probable relative error of 10%. Strictly speaking this N_H value should be considered as an upper limit since a circumstellar contribution to N_H cannot be ruled out. Jordan et al. (1994) have instead obtained a value for N_H in the range 1.7–3.1 $\times 10^{20}$ from ROSAT PSPC observations. The mean relations between neutral hydrogen column density and dust by Diplas & Savage (1994) ($N_H = 4.93 \times 10^{21}\ E_{(B-V)}$) gives $E_{(B-V)} = 0.014$, in good agreement with our estimates.

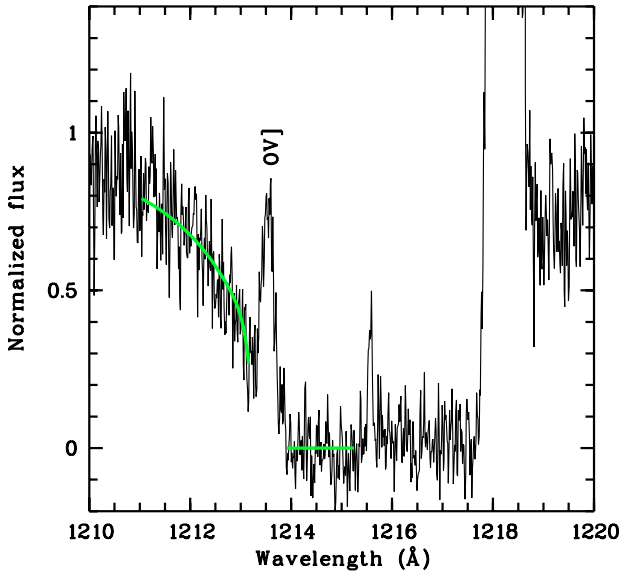

Fig. 5. The interstellar Lyα line. Our best fit to the damping wing, excluding the [O V] λ 1213.81 emission line, implies a hydrogen column density $N(\mathrm{H}) = 6.9 \times 10^{19}$ cm^{-2} and is shown as a solid line.

The HEASARC N_{H} tool (`heasarc.gsfc.nasa.gov/cgi-bin/Tools/w3nh/w3nh.pl`) in which N_{H} is derived from the HI map by Dickey & Lockman (1990) indicates a total galactic column density N_{H} in the direction of RR Tel very close to 4.5×10^{20} (atoms cm^{-2}). It should be pointed out, however, that the N_{H} tool gives the average value for 1 degree × 1 degree bins.

The valuable Web site "Galactic Dust Extinction Service" (`http://irsa.ipac.caltech.edu/applications/DUST/`) employs the 100-micron intensity map of the sky by Schlegel et al. (1998) to provide the foreground (Milky Way) extinction for a line of sight and/or region of the sky. This tool gives $E_{(B-V)} = 0.05$ as the total extinction in the line of sight of RR Tel. The spatial resolution of the map is higher than for N_{H} (about 5 arcmin) but, as clearly stated in the cautionary notes, the various assumptions made in the conversion from the 100-micron dust column density to the color excess $E_{(B-V)}$ may affect the resulting $E_{(B-V)}$ value.

3.4. Comments on the reddening

The observations described in the previous sections have convincingly shown that $E_{(B-V)} \sim 0$.

We recall that previous $E_{(B-V)}$ values in the literature range from values as high as 0.7, estimated by Walker (1977) from the Balmer decrement, to values close to 0.08–0.10, (Penston et al. 1983; Feast et al. 1983; Jordan et al. 1994; Espey et al. 1996), down to values close to zero (Glass & Webster 1973). The generally accepted $E_{(B-V)}$ values in the literature are in the range 0.08–0.10. Recently, Pereira et al. (1999), using ESO data with spectral resolution of ∼2.5 Å (*FWHM*) have obtained $E_{(B-V)} = 0.04$ from the relative ratios of $\mathrm{H}_\gamma/\mathrm{H}_\beta$, $\mathrm{H}_\delta/\mathrm{H}_\beta$ and He II 3203/4686. Very recently, Young et al. (2005) have derived $E_{(B-V)} \leq 0.28$ from a study of the Fe VII lines, based on the same STIS and UVES spectra of RR Tel as this work. The authors have pointed out, however, that the extinction is not well constrained by the Fe VII lines and have derived $E_{(B-V)} \sim 0.11$ from the comparison of the observed and the theoretical (Galavis et al. 1997) NeV I_{2974}/I_{1574} line ratio.

We therefore emphasize that the $E_{(B-V)}$ value obtained in the present study with the method of the He II Fowler lines is based on data from 20 lines and is extremely well constrained, because of the wide wavelength coverage of the lines and because of the fact that most of them fall close to the region near λ 2200, where the maximum of the extinction occurs. Moreover, if, as an exercise, the observed STIS continuum plotted in Fig. 3 were "dereddened" assuming $E_{(B-V)} = 0.10$, the resulting continuum would show an artificial emission bump near λ 2000.

3.5. The distance to RR Tel

The photometric and spectral development of RR Tel during the OB phases was that of an extremely slow nova that was near maximum between the end of 1944, when the outburst occurred, until June 1949 (Friedjung 1974; Heck & Manfroid 1985). It seems therefore reasonable to assume that the nova luminosity was near-Eddington during these decay phases. For a WD mass near 0.6 $M_\odot$, as expected in an extremely slow nova (Livio 1992), this assumption gives $M_{\mathrm{Bol}}^{\mathrm{max}} \sim -6.1$, and assuming a bolometric correction BC ~ -0.1 for an object with $T \leq 10\,000$ K, we obtain $M_v^{\mathrm{max}} = -6.0$, in good agreement with the estimates from the various relations (Della Valle & Livio 1995; Downes & Duerbeck 2000) between the absolute magnitude at maximum and the rate of decline (MMRD).

From the observed $m_v^{\mathrm{max}} = 6.7$ and our new value for the extinction ($A_v = 0.0$) a distance of 3.47 kpc is obtained.

This value is in good agreement with that of 3.6 kpc obtained by Feast et al. (1983) on the assumption that a Mira is present in RR Tel. Whitelock (1988) has instead derived $d \sim 2.6$ kpc by applying a period-brightness relation to the IR magnitudes and the pulsation period of the Mira in the system.

From our estimated distance ($d = 3.47$ kpc) and the total IS hydrogen column density derived from the Ly-α damped profile ($N_{\mathrm{H}} = 6.9 \times 10^{19}$ atoms cm^{-2}) one obtains that the average hydrogen number density $N(\mathrm{H})$ (atoms cm^{-3}) is $\sim 6.7 \times 10^{-3}$. We recall that Diplas & Savage (1994) found limits of 0.017–8.62 for the hydrogen number density in the galactic ISM. Therefore, the intervening ISM towards RR Tel seems extremely poor in the content of dust and neutral hydrogen.

4. The O III Bowen lines

4.1. The O III Bowen fluorescence mechanism

In high-excitation planetary nebulae and symbiotic stars a significant fraction of the EUV – soft X-ray flux (at wavelengths shortward of the He II Lyman limit, $h\nu \geq 54.4$ eV) is absorbed by the nebula and converted into the He II Ly-α λ 303.782 emission line that may then attain a high intensity. These λ 303.782 photons can ionize both H and He and therefore they have a strong influence on the ionization and temperature structure of the nebula.

Scattering of these He II Ly-α resonance photons may result in one of the following processes (See Aller 1984; Osterbrock & Ferland 2006): 1) escape from the nebula by diffusion in the wings, 2) photoionization of He° and H, 3) absorption by O III: in a near coincidence in wavelength with the λ 303.800 resonance transition of O III the He II Ly-α λ 303.782 photons may excite its 2p3d ^{3}P$_2$ level at 40.85 eV (O1 process).

The most likely radiative process from the excited 2p3d ^{3}P$_2$ level of O III (total probability about 0.98 = 0.74+0.24) is that of resonant scattering, by emission of one of the two resonance lines at lambda 303.800 (2p3d ^{3}P$_2$–2p^2 ^{3}P$_2$) (O1 line) and lambda 303.622 (2p3d ^{3}P$_2$–2p^2 ^{3}P$_1$) (O2 line).

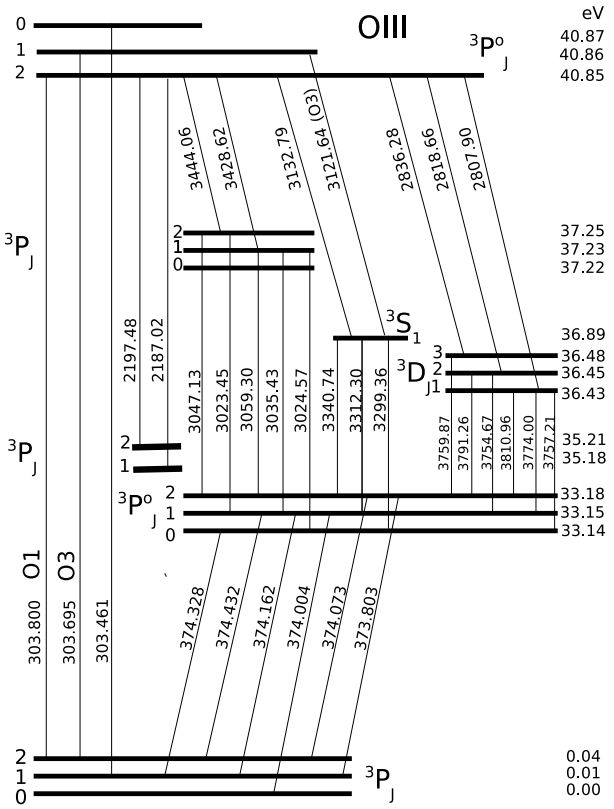

Fig. 6. A partial Grotrian diagram of O III that includes the most relevant O1 transitions and the λ 3121.64 line belonging to the O3 process. The level's configuration can be read from Table 3. The y-axis is not scaled linearly.

Table 3. Configuration and energy of the relevant O III Bowen fluorescence levels.

Level	E(eV)	E(cm^{-1})
2p3d $^3P^\circ_0$	40.87	329 645.14
2p3d $^3P^\circ_1$	40.86	329 583.89
2p3d $^3P^\circ_2$	40.85	329 469.80
2p3p $^3P_2$	37.25	300 442.55
2p3p $^3P_1$	37.23	300 311.96
2p3p $^3P_0$	37.22	300 239.93
2p3p $^3S_1$	36.89	297 558.66
2p3p $^3D_3$	36.48	294 223.07
2p3p $^3D_2$	36.45	294 002.86
2p3p $^3D_1$	36.43	293 866.49
2p^4 $^3P_1$	35.21	283 977.4
2p^4 $^3P_2$	35.18	283 759.7
2p3s $^3P^\circ_2$	33.18	267 634.00
2p3s $^3P^\circ_1$	33.15	267 377.11
2p3s $^3P^\circ_0$	33.14	267 258.71
2s2p^3 $^3S^\circ_1$	24.44	197 087.7
2s2p^3 $^3P^\circ_0$	17.65	142 393.5
2s2p^3 $^3D^\circ_1$	14.88	120 058.2
2s2p^3 $^3D^\circ_2$	14.88	120 053.4
2s2p^3 $^3D^\circ_3$	14.88	120 025.2
2p^2 $^3P_2$	0.04	306.17
2p^2 $^3P_1$	0.01	113.18
2p^2 $^3P_0$	0.00	0.00

A less probable decay process from the aforesaid 2p3d^{3}P$_2$ level (total probability about 1.85%) is the cascade through the high lying 2p3p ^{3}P ($E \sim$ 37.23 eV), 2p3p ^{3}S ($E \sim$ 36.89 eV) and 2p3p ^{3}D ($E \sim$ 36.45 eV) terms, by emission of one of six subordinate lines (the primary cascade-decays) in the near-UV optical region of the spectrum (from λ 2807.90 to λ 3444.06). However, despite the low probability of the decay channel through the subordinate lines, if the optical depth in the He II Ly-α line is very high the trapped He II Ly-α photons are repeatedly scattered and a significant fraction of them can be converted into the fluorescent cascade of optical and ultraviolet lines. Unlike the resonance and near resonance lines that are scattered many times, the photons produced by these subordinate transitions can easily escape from the nebula, and, together with the subsequent cascades (the "secondary" decays), that produce additional emission lines, (most of them in the optical U spectral range), comprise the Bowen fluorescence lines (Bowen 1934).

Figure 6 represents a partial Grotrian diagram of O III that includes the most common Bowen O1 transitions. Figure 6 is complemented by Table 3 that includes the configuration and the energy (eV and cm^{-1}) of the relevant levels.

In most planetary nebulae and symbiotic stars, the "efficiency" of the Bowen mechanism, that is the fraction of He II Ly-α photons that is converted into O III Bowen lines (mostly a function of the He II Ly-α optical depth) varies from object to object and covers almost the whole range of possible values (Liu & Danziger 1993; Pereira et al. 1999). Therefore, the Bowen mechanism can have a major influence on the fate of the He II Ly-α photons and consequently also on the photoionization equilibrium in the nebula. Thus, a clear understanding of the Bowen mechanism is required for a correct interpretation of the emergent UV and optical spectrum.

If the width of the He II Ly-α line is large enough, an additional fluorescence process might also be present i.e. the excitation of the O III (2p3d)^{3}P$_1$ level ($v = -82$ km s^{-1} from He II λ 303.782) due to the partial overlap of the exciting He II Ly-α with the λ 303.695 resonance line of O III (O3 process). In addition, if He II Ly-α is even wider, then excitation of the (2p3d)^{3}P$_0$ level by pumping in the resonance line at λ 303.461 could also take place. This is a quite uncommon process, since this line is at -250 km s^{-1} with respect to He II Ly-α. Thus, these two secondary Bowen fluorescence processes provide a convenient probe which measures the intensity of radiation in the far wings of the unobserved He II Ly-α line and gives valuable information on its width. It is worth recalling that Bhatia et al. (1982) in a study of the solar O III spectrum have pointed out the fact that the He II Ly-α line is considerably broader than the O III lines.

It is important to note that while the lines in the primary cascade from each (2p3d)^{3}P$_{0,1,2}$ level are individual, (e.g. λ 3132.79 from (2p3d)^{3}P$_2$ (O1), λ 3121.64 from (2p3d)^{3}P$_1$ (O3), λ 3115.68 from (2p3d)^{3}P$_0$) most of the lines in the subsequent cascades are common to the three processes, although the dominant contribution comes from the O1 process.

We recall that a competitive charge-exchange mechanism (CE) functions for some of the lines produced in the decay from the ^{3}D term (Dalgarno & Sternberg 1982), while the λ 5592.25 line (3s ^{1}P°–3p ^{1}P, mult. 5) comes from charge-exchange only (see Liu & Danziger 1993 and Kastner & Bhatia 1996, hereinafter KB96 for details).

An accurate determination of the intensities of the pure Bowen lines is fundamental for determining the relative contribution by the various channels previously mentioned. KB96 have pointed out that a complete Bowen system has not yet been observed because of inadequate coverage in wavelength, lack of adequate spectral resolution, lack of accurate ELI, and

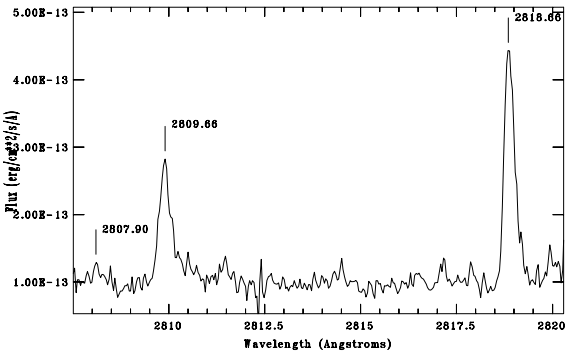

Fig. 7. The weak O III Bowen lines near λ 2800 in STIS.

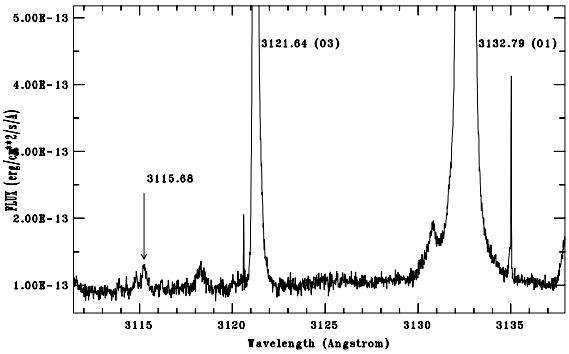

Fig. 8. The UVES spectrum shows the strongest line of each of the three Bowen excitation channels. *From left to right*: the very weak λ 3115.68 line (from 2p3d $^3P_0$, at −250 km s^{-1} from He II Ly-α), the O3 λ 3121.64 line (from 2p3d $^3P_1$, at −88.2 km s^{-1} from He II Ly-α), and the strong O1 λ 3132.79 line (from 2p3d $^3P_2$, at +16.4 km s^{-1} from He II Ly-α).

lack of overlap between the data of various observers. Also, the lack of sufficiently accurate intensities for the weak CE line at λ 5592.25, and for the primary cascade line of the O3 process at λ 3121.64 is particularly relevant, according to KB96.

4.2. The Bowen lines intensities in RR Tel

In our UVES data (spectral resolution ∼0.05 Å *FWHM*) we have detected and measured all of the O III fluorescent lines (O1 and O3 processes) that are present in the range $\lambda\lambda$ 3047–3811, with the sole exception of the two lines at λ 3759.87 and at λ 3810.96 that are blended with stronger lines of [Fe VII] λ 3758.92 and O VI(1) λ 3811.35, respectively. The remaining lines are unblended except for the λ 3405.71 line which is partially affected by the presence of the λ 3405.78 O IV(3) line.

Figures 7 and 8 are self-explanatory and illustrate the exceptional quality of the STIS-NUV-MAMA and UVES spectral data that have allowed the detection and measurement of the pure lines produced in the various Bowen excitation processes, including the very weak λ 3115.68 line that is associated with the excitation of the $(2p3d)^3P_0$ level by the He II λ 303.461 line.

The STIS data are complementary to the UVES data shortward of λ 3047 (see also Fig. 9) and include all of the Bowen lines present in this range, although the two lines at λ 2807.90 and λ 2798.90 are very weak. In the spectral range that is common with UVES (longward of λ 3046) the STIS data include most of the Bowen lines detected by UVES except the weakest ones that have not been detected because of lower spectral

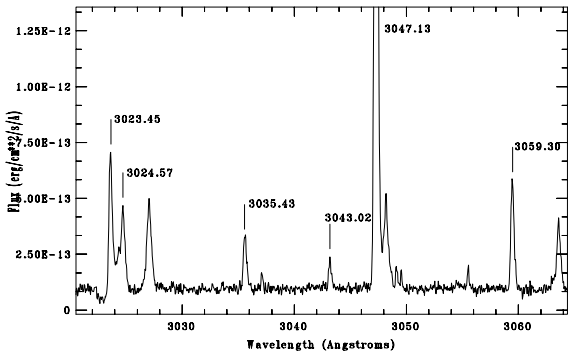

Fig. 9. The weak O III Bowen lines in the STIS region near λ 3030.

resolution and S/N in the STIS optical data compared with that of UVES.

The merging of the STIS and UVES data (as mentioned in Sect. 2) has thus provided a high quality coverage of ELI for almost all of the O III Bowen lines in the range $\lambda\lambda$ 2798–3810.

Table 4 gives the observed STIS and UVES ELI (10^{-13} erg cm^{-2} s^{-1}) and their ratios with respect to the reference line λ 3444.06. The wavelengths and the radiative rates A_{ij} are from KB96, that adopted the IC rates of Froese Fisher (1994). It should be noted that these values differ by about 10%, with nearly constant ratio, from those listed in the NIST Web site, whose accuracy is in the range C (≤25%) – C$^+$ (≤18%). Therefore, the level branching ratios are nearly the same, and the detailed discussion of the decays (see also Sect. 4.6) is not affected. We note, incidentally, that the λ 2808.77 line in KB96 should be correctly reported as λ 2807.90. In this list we have also included for comparison the CE process line at λ 5592.25, the hydrogen H$_\beta$ line λ 4861, and the He II Ba-α λ 1640, Pa-β λ 3203 and Pa-α λ 4685.71 lines. The *FWHM* values (deconvolved from the instrumental *FWHM*) are from STIS in the UV region (shortward of λ 3044) and from UVES in the optical region, with the only exception of the *FWHM* of He II λ 4686 that is from STIS. The last column of Table 4 gives the number of photons in the line, obtained from the observed ELI after proper conversion.

As mentioned in Sect. 2.2, the intensity ratios for the lines that are common to the two sets of measurements are in good agreement with mean value =1.16 and variation coefficient =2.9%. The consistency between the two sets of data lend support to the re-calibration method adopted for UVES and to the overall correctness of the method.

It should be pointed out that in an earlier short study based only on UVES data (Selvelli & Bonifacio 2001) the values for the relative emission intensities were slightly different since the UVES calibration was based on standard ground-based reduction method, and the correction for the color excess was assumed to be $E_{(B-V)} = 0.10$. However, only for the λ 5592.25 line is the difference with the previous measurements significant.

The I_{3133}/I_{3444} ratio in STIS data is =3.18, and, consistently =3.11 in UVES data. The same ratio was reported as =3.39 by Pereira et al. (1999), in a study of Bowen fluorescence lines for a group of symbiotic stars, including RR Tel using ESO data with spectral resolution of ∼2.5 Å (*FWHM*). As mentioned in Sect. 3.4 they have adopted $E_{(B-V)} = 0.04$.

In conclusion, we have obtained high quality data for about thirty O III lines of the Bowen fluorescence process, including six pure O1 lines ($\lambda\lambda$ 2807.90, 2818.66, 2836.28, 3132.79, 3428.62 and 3759.87), seven pure O3 lines

Table 4. Bowen fluorescence lines. The nine colums give: the laboratory wavelengths (Å, in air), the transition, the A_{ij} (s^{-1}) (from KB96, except for the first two lines taken from "The Atomic Lines List 2.05" (`http://www.pa.uky.edu/~peter/newpage`); 1.48e+8 represents $1.48 \times 10^{+8}$), the line *FWHM* (km s^{-1}), the ELI (10^{-13} erg cm^{-2} s^{-1}) from STIS and UVES data, the relative ELI $STIS_r$ and $UVES_r$ ($I_{3444.06}$ = 100), and the photon number N_v (in 10^{-3} photons cm^{-2} s^{-1}) from the STIS scale.

λ_{air}	Transition	A_{ij}	*FWHM*	STIS	UVES	$STIS_r$	$UVES_r$	N_v
2187.02	3d $^3P^\circ_2$–2p^4 $^3P_2$	7.19+5	(41.3)	0.40	–	1.24	–	4.41
2197.48	3d $^3P^\circ_2$–2p^4 $^3P_1$	2.36+5	(40.5)	0.21	–	0.65	–	2.32
2798.90	3d $^3P^\circ_1$–3p $^3D_1$	3.14+6	–	(0.05)	–	(0.15)	–	(0.70)
2807.90	3d $^3P^\circ_2$–3p $^3D_1$	1.79+5	–	(0.03)	–	(0.1)	–	(0.42)
2809.66	3d $^3P^\circ_1$–3p $^3D_2$	1.41+7	(39.3)	0.65	–	2.02	–	9.21
2818.66	3d $^3P^\circ_2$–3p $^3D_2$	1.57+6	33.0	1.12	–	3.48	–	14.47
2836.28	3d $^3P^\circ_2$–3p $^3D_3$	1.64+7	35.7	12.20	–	37.89	–	174.19
3023.45	3p $^3P_2$–3s $^3P^\circ_1$	5.17+7	37.1	2.37	–	7.36	–	36.07
3024.57	3p $^3P_1$–3s $^3P^\circ_0$	6.73+7	(43.5)	1.71	–	5.31	–	26.04
3035.43	23p $^3P_1$–3s $^3P^\circ_1$	5.06+7	34.1	0.87	–	2.70	–	13.29
3043.02	3p $^3P_0$–3s $^3P^\circ_1$	2.14+8	28.6	0.37	–	1.15	–	5.66
3047.13	3p $^3P_2$–3s $^3P^\circ_2$	1.63+8	34.8	15.30	13.91	47.52	49.86	234.70
3059.30	3p $^3P_1$–3s $^3P^\circ_2$	9.46+7	34.5	1.74	1.44	5.40	5.16	26.80
3115.68	3d $^3P^\circ_0$–3p $^3S_1$	1.41+8	36.4	–	(0.11)	–	(0.39)	(2.04)
3121.64	3d $^3P^\circ_1$–3p $^3S_1$	1.44+8	27.9	3.67	3.25	11.40	11.63	57.65
3132.79	3d $^3P^\circ_2$–3p $^3S_1$	1.52+8	34.6	102.4	86.9	318.0	311.5	1615.1
3299.36	3p $^3S_1$–3s $^3P^\circ_0$	1.79+7	34.2	4.32	3.66	13.42	13.12	71.76
3312.30	3p $^3S_1$–3s $^3P^\circ_1$	4.97+7	34.1	11.40	9.50	35.40	34.05	190.01
3340.74	3p $^3S_1$–3s $^3P^\circ_2$	6.84+7	34.1	15.10	12.85	46.89	46.09	253.90
3405.71	3d $^3P^\circ_1$–3p $^3P_0$	1.78+7	28.9	–	0.40	–	1.43	8.23
3408.12	3d $^3P^\circ_0$–3p $^3P_1$	7.27+7	25.3	–	(0.04)	–	(0.14)	(0.85)
3415.26	3d $^3P^\circ_1$–3p $^3P_1$	2.31+7	27.8	–	0.49	–	1.76	10.31
3428.62	3d $^3P^\circ_2$–3p $^3P_1$	7.98+6	38.2	4.74	3.78	14.72	13.55	81.79
3430.57	3d $^3P^\circ_1$–3p $^3P_2$	2.78+7	26.7	(0.60)	0.55	(1.86)	1.97	10.38
3444.06	3d $^3P^\circ_2$–3p $^3P_2$	5.21+7	34.9	32.20	27.90	100.0	100.0	558.25
3754.67	3p $^3D_2$–3s $^3P^\circ_1$	8.67+7	31.8	(0.77)	1.05	(2.39)	3.76	14.55
3757.21	3p $^3D_1$–3s $^3P^\circ_0$	6.42+7	33.5	(0.25)	0.24	(0.78)	0.86	4.73
3759.87	3p $^3D_3$–3s $^3P^\circ_2$	1.13+8	–	bl	bl	bl	bl	–
3774.00	3p $^3D_1$–3s $^3P^\circ_1$	4.55+7	30.7	(0.28)	0.22	(0.87)	0.79	5.23
3791.26	3p $^3D_2$–3s $^3P^\circ_2$	2.61+7	35.4	–	0.30	–	1.08	6.87
3810.96	3p $^3D_1$–3s $^3P^\circ_2$	2.79+6	–	–	–	–	–	–
5592.25	3s $^1P^\circ$–3p ^1P	–	37.3	–	0.12	–	0.44	4.05
He II-3203	3–5	–	54.2	63.5	54.65	197.2	195.9	1023.9
He II-4686	3–4	–	56.2	147.5	–	458.0	–	3477.9
He II-1640	2–3	–	63.2	831.0	–	2580.7	–	6860.4
HI-4861	2–4	–	60.0	162.0	–	503.1	–	3964.7

($\lambda\lambda$ 2798.90, 2809.66, 3043.02, 3121.64, 3405.71, 3415.26, and 3430.57) and the two pure very weak lines at λ 3115.68 and λ 3408.12 that come from the pumping of level 2p3d $^3P^\circ_0$ (40.87 eV) which requires a very wide He II Ly-α line (this process is called "other" in KB96). It is worth recalling (see also KB96) that these two lines were reported (but not measured) in the comprehensive paper on RR Tel by Thackeray (1977). The λ 3115.68 line was correctly identified as O III, while the λ 3408.12 line was tentatively identified as a CrII line.

4.3. The Bowen lines width and profile

The data for the *FWHM* for the O III Bowen lines reported in Table 4 (obtained from the high resolution spectra of STIS and UVES) give an average *FWHM* value of 34.30 ± 1.90 km s^{-1} for the O1 + mixed (O1+O3) lines, while the average *FWHM* for the five best observed pure O3 lines is =27.98 ± 0.85 km s^{-1}. The difference is significant with a ratio *FWHM*(O1)/*FWHM*(O3) ~ 1.22.

It is also remarkable that in UVES spectra all the best observed O III Bowen lines (i.e. λ 3133, λ 3121, λ 3299, λ 3312, λ 3340, λ 3444, etc.) show a definite asymmetry (excess) in the red wing (see Fig. 10). The red "excess" (after subtraction of the main Gaussian component of about 34.3 km s^{-1} *FWHM*) can be modeled by a Gaussian profile centered at about +38 km s^{-1} from the main component and with *FWHM* of about 22 km s^{-1}. There is however still an "excess" left and the velocity profile in the "red" wing can reach a maximum velocity of ~100 km s^{-1}. Alternatively, the entire profile can be also (and better) fitted with a Gaussian main component with *FWHM* 31 km s^{-1} m, while the red "excess" is represented by a Voigt profile with *FWHM* 25 km s^{-1} in the Gaussian core and 17 km s^{-1} in the Lorentzian wing.

A similar but less enhanced behavior is shown by the He I lines at λ 5875, and λ 6678, while the two [O I] lines at λ 6300 and λ 6363 show two almost resolved components with separation of 27 km s^{-1} and *FWHM* of 13 km s^{-1} and 28 km s^{-1} respectively.

Surprisingly, the nebular [O III] lines at λ 4958 and λ 5007 show instead an excess in the blue wing with a maximum velocity of about −150 km s^{-1}, while other strong emission lines observed with UVES e.g.: He II λ 3203, [Ne V] λ 3426, [Fe VII] λ 3586, H-β λ 4861, [Fe VII] λ 4893, [Ca VII] λ 4939, [Fe VII] λ 5176, He II λ 5411, [Ca VII] λ 5618, [Fe VII] λ 5721,

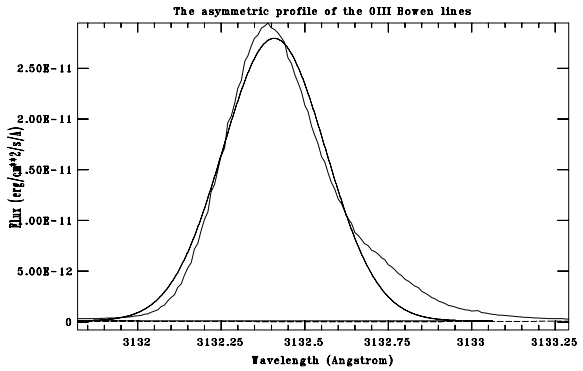

Fig. 10. The asymmetric profile of the O III λ 3133 line and a Gaussian fit with $FWHM$ = 34.5 km s^{-1}. The same kind of profile is present also in other lines, see Sect. 4.3.

[Fe VII] λ 6086, [Ar V] λ 6434, and [Ar V] λ 6455 show an almost pure Gaussian profile.

We recall that Crawford (1999) reported the presence of a two component structure in the [O III] λ 4363 line and of a multi-component structure in the [O III] λ 4959 and λ 5007 lines. Schild & Schmid (1996) also observed this behavior and attributed it to the presence of two nebular components of different densities.

In the far UV and near UV echelle spectra of STIS (taken 1 year after the UVES spectra) whose resolution is comparable to that of UVES, a red wing excess similar to that present in λ 3132.79 is present in all of the common intercombination lines, e.g. O V] λ 1218, O IV] λ 1404, N IV] λ 1486, O III] λ 1660 and λ 1666, N III] λ 1750, Si III] λ 1892 and C III] λ 1906. It is instead absent in the lines of permitted transitions, i.e. in the three resonance doublets of N V (λ 1238, λ 1242), SiIV (λ 1293, λ 1403), and C IV (λ 1548, λ 1550) and in the He II Ba-α recombination line λ 1640, all of which display a nearly pure Gaussian profile.

The asymmetry is not evident in the STIS optical [O III] lines possibly because of the lower spectral resolution of STIS in the optical range. In FEROS spectra, in the range outside that covered by UVES, there is evidence of excess in the [O III] λ 4363 nebular line (as mentioned by Crawford 1999), and in the O I λ 8446 line produced by the Ly-β fluorescence. No excess is evident in H$_\gamma$ λ 4340, and in He II λ 4686.

4.4. The relative Bowen line intensities and the efficiency of the O1 and O3 processes

The high quality of the data has allowed a detailed comparison of the observed ratios for pairs of lines from a common upper level to the corresponding branching ratios obtained from the transition rates given by Bhatia & Kastner (1993) (BK), Froese Fischer (1984) (FF), and Saraph & Seaton (1980) (SS).

Following Pereira et al. (1999) we present in Table 5 a comparison between the observed and the predicted ratios for some selected lines. It is clear from Table 5 that the best agreement in the overall ratios is with the Froese Fisher (1994) model. This strongly supports the intermediate coupling radiative rates calculated by FF.

The efficiency of the Bowen fluorescence mechanism is quantified by the fraction of the created He II Ly-α photons (λ 303.782) that are converted into Bowen line photons. If the atomic transition probabilities are known, the intensity of any He II line can be related to the intensity of the He II Ly-α line

Table 5. A comparison between observed and predicted intensity ratios for pairs of Bowen lines originating from the same upper level. The theoretical intensity ratios have been derived from the transition rates of Bhatia & Kastner (1993) (BK), Froese-Fisher (1994) (FF), and Saraph & Seaton (1980) (SS).

line ratios	STIS	UVES	BK	FF	SS
2819/3444	0.035	–	0.033	0.037	–
2836/3444	0.38	–	0.43	0.38	–
3133/3444	3.18	3.12	4.06	3.21	3.61
3429/3444	0.15	0.14	0.18	0.15	0.34
3406/3415	–	0.81	0.75	0.78	–
3415/3122	–	0.15	0.09	0.15	–
3299/3341	0.29	0.28	0.23	0.26	0.20
3299/3312	0.38	0.38	0.35	0.36	0.34
3791/3755	–	0.29	0.31	0.30	0.33

(and to the number of He II Ly alpha photons) and the intensity of any Bowen line can be related to the total intensity of the Bowen lines (and total number of Bowen photons). In this case, the efficiency can be easily calculated if the (relative) intensities of a single Bowen line (usually λ 3133 or λ 3444) and a single He II line (usually λ 4686, or λ 3203) are available. The efficiency factor R can be defined as:

$$R = \frac{P \cdot \alpha_{\rm eff}(4686) \cdot \lambda \cdot I_\lambda}{P_\lambda \cdot \alpha_{\rm eff}(304) \cdot 4686 \cdot I_{4686}}$$

where $\alpha_{\rm eff}(304)$ and $\alpha_{\rm eff}(4686)$ are the effective recombination coefficients for recaptures that result in the production of λ 304 and λ 4686 respectively, P is the cascade probability =0.0187, and P_λ is the probability for the emission of a particular Bowen line following the excitation of 2p3d ^{3}P$^\circ_2$ (O1) (Aller 1984). The ratio of the two $\alpha_{\rm eff}$ is 0.328 for $T_{\rm e}$ = 10 000 K.

The application to specific lines provides simple relations that can be directly used, i.e. $R \sim 1.0 \cdot I_{3444}/I_{4686}$ (Kaler 1967; Harrington 1972), $R = 0.12 \cdot I_{3133}/I_{3203}$ (Schachter et al. 1990), $R = 0.32 \cdot I_{3133}/I_{4686}$ (Saraph & Seaton 1980) $R = 0.43 \cdot I_{3444}/I_{3203}$ (Wallerstein 1991). In the specific case of RR Tel these relations give R = 0.22, 0.21, 0.22, and 0.22, respectively, in encouraging agreement.

Similar relations can be obtained for the efficiency of the O3 channel. Shachter et al. (1991) give

$$\frac{R_{\rm O3}}{R_{\rm O1}} = \frac{I_{3122} \cdot A_{3133} \cdot 3122}{I_{3133} \cdot A_{3122} \cdot 3133}$$

and for the specific case of RR Tel one obtains that the relative $R_{\rm O3}/R_{\rm O1}$ efficiency is ~0.038 (a value that is much lower than that, ~0.3, found by Shachter et al. 1991 for AM Her). Therefore, the efficiency of the O3 channel in RR Tel is close to 0.7%.

In RR Tel we have obtained the intensities of all the Bowen lines belonging to the primary cascade. This fortunate situation allows a direct counting of the number of Bowen photons observed in the 6 lines of the primary O1 channel (the λ 2808.77 line is not detected) and therefore a more direct estimate of the efficiency. The total intensity in the 6 lines of the primary O1 decay from level 2p3d ^{3}P$^\circ_2$ (O1) is of 152.7 $\times$ 10^{-13} erg cm^{-2} s^{-1} (from STIS data). This value, after proper conversion from energy to number of photons, corresponds to a total number of photons (decays) in the O1 primary cascade of approximately 2.45 photons cm^{-2} s^{-1} (see also Table 4).

The He II Ly-α intensity can be estimated from the observed λ 4686 line intensity (~147.5 $\times$ 10^{-13} erg cm^{-2} s^{-1}) assuming a ratio $I_{304}/I_{4686} \sim 65$ (Storey & Hummer 1995). The corresponding number of He II Ly-α photons is about 15.36 cm^{-2} s^{-1}. Thus,

the efficiency for the O1 channel R(O1) is close to 16.0%, with some uncertainty associated with the actual value of the He II Ly-α intensity.

We recall that the excitation of the 2p3d $^3P_1$ level of O III (the O3 channel) requires a velocity shift of -88.2 km s^{-1} from the rest wavelength of the He II Ly-α line, while the excitation of the 2p3d $^3P_0$ level (that produces the two very weak but observed lines at λ 3115 and λ 3408) requires a corresponding velocity shift of -250 km s^{-1}. This clearly indicates that the λ 303.782 He II Ly-α line must be broad enough to excite these levels of O III.

As reported in Sect. 3.1, the average *FWHM* for 20 unblended lines of the Fowler series is =53.5 ± 3.5 km s^{-1}. while the He II Ba-α line λ 1640 has *FWHM* = 63.2 km s^{-1}. These values are about ten times larger than the thermal velocities that are on the order of about 6.4 km s^{-1}.

It is clear from these values that the He II Ly-α line is much broader than the He II recombination lines, probably a consequence of multiple resonant scatterings.

4.5. The past efficiency of the O III Bowen fluorescence process

In most IUE LW high resolution spectra of RR it is possible to obtain good measurements for the He II Fowler lines at λ 2733 and λ 3203 and for the O III lines at λ 2836, λ 3047 and λ 3133 (O1 process) and the O III line at λ 3122 (O3 process). Since the IUE spectra cover about 17 years in the life of RR Tel one can thus follow the changes with time in the absolute and relative intensities of the He II and O III lines and estimate the corresponding changes in the Bowen efficiency. Table 6 gives the time variation from 1978 to 1995 for these lines, as obtained from measurements on more than 30 IUE spectra, together with the data for Oct. 10, 2000 from STIS (last line).

As already mentioned in Sect. 2.3, the data in Table 6 all come from a choice of good quality spectra. The data clearly show that starting from the first spectra secured in August 1978 until the last spectra of August 1995 there has been a steady decrease with time in all ELI.

The data have been fitted with both linear and power-law regression. The behavior with time of the two He II lines, that of the three O III O1 lines and that of the O III O3 line is described by different power-law indices (~-0.33, ~-0.97, and ~-1.48, respectively) but within each line group the indices are similar. Figure 11 is a log-log plot of the data with their power-law fittings (straight lines) for the 6 spectral lines listed in Table 6.

On average, with the power-law fit, the intensity of the He II lines (λ 2733 and λ 3203) has decreased by a factor about 1.5 from 1978 to 2000. Instead, the intensity of the O1 lines (λ 2836, λ 3047 and λ 3132) has decreased on the average by a factor larger than 3, and the O3 line (λ 3122) has decreased by a factor larger than 5.

Therefore, the efficiency in the O1 channel (as determined by the I_{3133}/I_{3203} ratio) from the power-law fitting was about 2.1 times higher in the early IUE years (1978–1980) and has decreased from a value near 0.5 in 1978–1980 to a value close to 0.2 in year 2000 (STIS). Similarly, the data indicate that the O3 efficiency has decreased more rapidly with time than the O1 efficiency and that in 1978–1980 the relative O3 over O1 efficiency was about two times higher than in 2000.

The O3 line is at -88.2 km s^{-1} from the He II Ly-α line. The higher relative efficiency O3/O1 in the past can be explained by a larger width in the He II Ly-α line, resulting from either a larger turbulence or larger optical depth effects in epochs closer to the outburst time. We attribute the decrease with time in the He II ELI to the general decrease in the luminosity of the central source (Murset & Nussbaumer 1993). The corresponding stronger decline in the O III Bowen lines indicates a gradual decrease in the Bowen efficiency (in particular for the O3 lines).

Table 6. The intensity (in 10^{-13} erg cm^{-2} s^{-1}) of the He II and O III emission lines from IUE high resolution spectra and STIS. MJD is the Modified Julian Date = JD – 2 400 000.5.

IUE image	MJD	λ2733	λ 2836	λ3047	λ3122	λ3133	λ3203
LWR02021	43728	695	684	633	330	4610	1520
LWR02995	43833	700	520	742	273	4345	1398
LWR03888	43932	762	594	627	255	3965	1133
LWR07536	44329	593	398	619	255	3715	1091
LWR07663	44363	667	526	603	254	4239	1157
LWR08234	44433	698	518	639	282	4203	1213
LWR08272	44437	681	562	631	247	3987	1370
LWR09238	44548	650	454	635	210	3802	1029
LWR10364	44710	570	508	479	210	3553	1032
LWR11293	44827	669	480	605	162	4268	1187
LWR11296	44827	687	436	618	238	4348	1141
LWR11744	44887	672	495	629	196	3147	1140
LWR14466	45265	632	486	610	181	3792	1432
LWP01664	45229	668	473	537	172	3963	1167
LWR16181	45503	564	411	471	181	3464	1003
LWP03001	45780	619	475	460	173	3753	1051
LWP08178	46561	629	419	429	170	3313	1088
LWP08180	46562	578	459	460	155	2876	1074
LWP08728	46635	602	378	425	128	2940	1136
LWP08729	46636	575	379	408	141	3260	1156
LWP10919	46951	617	391	409	131	2990	1118
LPW13770	47374	566	329	326	95	2197	1042
LWP20538	48414	541	343	293	86	2110	1107
LWP23569	48826	483	276	301	88	2022	1100
LWP24278	48932	567	268	319	85	1970	835
LWP25953	49188	606	284	354	81	2078	1055
LWP25954	49188	598	288	335	106	2225	916
LWP28078	49479	583	298	334	84	2238	1030
LWP29189	49611	586	273	297	96	2030	939
LWP30848	49872	561	320	290	90	1964	1030
LWP30849	49872	516	229	286	72	1884	874
LWP31348	49953	548	278	241	59	1767	979
STIS	51827	323	122	155	37	1024	635

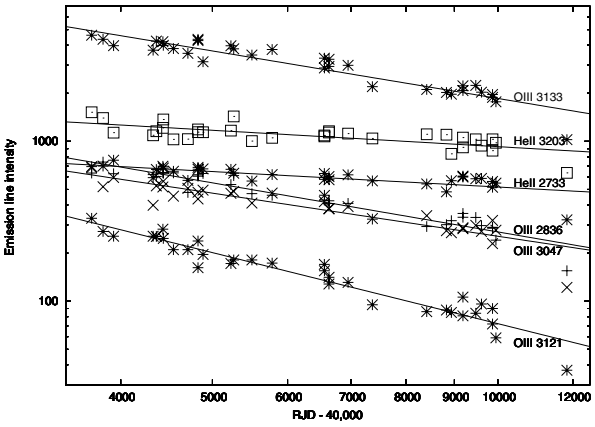

Fig. 11. A log-log plot of the decrease with time of the ELI of the He II and O III lines from 1978 to 1995 in IUE spectra. The last data are from STIS (Oct.10, 2000). The ELI are in units of 10^{-13} erg cm^{-2} s^{-1}. The power-law fits to the data (straight lines) have indices ~-0.33, ~-0.97, and ~-1.48, for the two He II lines (λ 2733 and λ 3203), the three O III O1 lines (λ 2836, λ 3047 and λ 3132), and the O III O3 line (λ 3122), respectively.

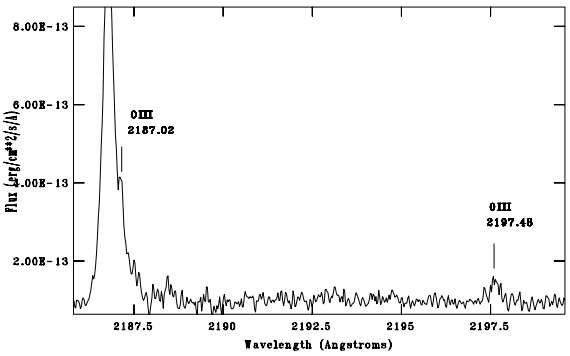

Fig. 12. Two "new" Bowen lines from the primary decay (40.85 eV). The λ 2187.02 line falls on the wings of the He II Fowler line λ 2186.60, while the λ 2197.48 line is weak but unblended. All wavelengths are in air.

This might be caused by a decrease in the width of the He II Ly-α profile together with a decrease in the optical depth of the O III resonance lines.

4.6. A detailed examination of the Bowen decays

In this section all of the transitions that enter and exit each energy level involved in the Bowen O1 fluorescence process are examined in detail in order to verify the balance in the number of photons (see Fig. 6, Tables 3 and 4). The lists of lines that enter or exit the relevant levels and their A_{ij} values have been obtained with the help of the extensive compilation of levels and transitions by van Hoof in the "The Atomic Line List 2.05" (`http://www.pa.uky.edu/~peter/newpage`).

1. The 2p3d $^3P^\circ_2$ level (40.85 eV, 329 469.80 cm^{-1}), is pumped directly by the He II Ly-α λ 303.782 line. The list of all primary decays from this level includes, (besides the two resonance lines λ 303.800 and 303.622) the 6 lines at $\lambda\lambda$ 2807.90, 2818.66, 2836.28, 3132.79, 3428.62, and 3444.06, and two additional lines (with rather low A_{ij} values) at λ (air) 2187.02 ($I = 0.40 \times 10^{-13}$ erg cm^{-2} s^{-1}) and at λ (air) 2197.48 ($I = 0.21 \times 10^{-13}$ erg cm^{-2} s^{-1}) that correspond to decays from 2p3d $^3P^\circ_2$ down to 2p^4 $^3P_2$ and 2p^4 $^3P_1$ at 35.18 and 35.21 eV, respectively. These two lines, albeit weak, have been detected in STIS spectra. The λ 2187.70 line falls in the wing of the He II Fowler line λ 2187.28 but is clearly present, while the other line at λ 2198.17 is weak but unblended (Fig. 12). To the best of our knowledge they have never been reported so far in any astronomical source.
   For lines that come from the same upper level k, the relative photon numbers are proportional to the respective A_{jk}. From the data in Table 4 we note that the observed photon number for the six lines of the primary decay (see also Fig. 6) are in good agreement with the the A_{jk} transition rates.
2. The 2p3p$^3P_2$ (300 442.55 cm^{-1}, 37.25 eV) and the 2p3p$^3P_1$ (300 311.96 cm^{-1}, 37.23 eV) levels are populated by the λ 3444.06 and the λ 3428.62 decays, respectively (from 2p3d $^3P^\circ_2$).
   Decays from these two levels include the five observed lines at $\lambda\lambda$ 3023.45, 3047.13, 3024.57, 3035.43, and 3059.30 (total $A_{ij} = 3.99 \times 10^8$) and five EUV lines with lower term 2s 2p^3 $^3D^\circ_{1,2,3}$ near λ 554.5 (total $A_{ij} = 2.36 \times 10^8$), plus other weaker decays.
   From the relative A_{ij} values one would expect that the contribution by the EUV lines should be about 0.67 of that of the observed near-UV lines (in the number of decays). The total number of decays in the two parent lines (λ 3428.62 and λ 3444.06) is =640.0 $\times$ 10^{-3} s^{-1} (Table 4). The same quantity for the five subsequent lines at $\lambda\lambda$ 3047.13, 3023.45, 3059.30, 3035.43, 3024.57 amounts to 337.1 $\times$ 10^{-3} cm^{-2} s^{-1}. Therefore there is an apparent (moderate – about 12%) deficiency of decays in these five observed transitions, if the A_{ij} values are accurate.
   Inspection of the other possible transitions listed in the "Atomic Line list 2.05″ shows that, besides some forbidden transitions, there are two additional decays from 2p3p$^3P_1$ and 2p3p$^3P_2$ down to 2s2p^3 $^3S^\circ_1$ (197 087.70 cm^{-1}, 24.44 eV), via λ 968.76, and λ 967.54 respectively (mult. UV 17.05), whose A_{ij} values are close to 1.24e+06, that is, about 1% of those of the five lines above. These lines are also reported in Table 7 of Saraph & Seaton (1980). However, inspection of BEFS spectra taken in Nov. 1996 has not led to their detection.
3. The 2p3p$^3S_1$ level (297 558.66 cm^{-1}, 36.89 eV).
   This level is important because it is fed by λ 3132.79, the strongest primary line in the decay from 2p3d $^3P^\circ_2$ (the O1 process). It is fed also by λ 3121.64, the strongest primary line in the decay from 2p3d $^3P^\circ_1$ (O3 process) and by λ 3115.68, the strongest decay from 2p3d$^3P^\circ_0$, but the contribution from this latter line is almost negligible.
   From the data of Table 4 we note that there is a severe unbalance between the total number of photons in the $\lambda\lambda$ 3132.79 and 3121.64 lines (=1674.0 $\times$ 10^{-3} cm^{-2} s^{-1}) and the corresponding quantity (=515.7 $\times$ 10^{-3} cm^{-2} s^{-1}) for the three observed subsequent decay transitions at $\lambda\lambda$ 3340.74, 3312.30, and 3299.36.
   Inspection of "The Atomic Lines List 2.05" and of the relevant radiative rates (A_{ij}) shows that additional decays from 2p3p$^3S_1$ that could contain the missing photons pass through 2s2p^3 $^3P^\circ_j$ ($J = 0, 1, 2$) (142 381.0, 142 381.8, and 142 393.5 cm^{-1}, ~17.65 eV) with three lines that fall close to λ 644.44 (mult. UV 16.20). The sum of the A_{ij} values of these λ 644.44 lines is larger by a factor 2.5 relative to that of the three optical lines. In other words, about 71% of the decay photons go into the three lines near λ 644, thus reconciling the inbalance in the number of decays. The expected intensity of the λ 644 lines with respect to that (~31.0 $\times$ 10^{-13} erg cm^{-2} s^{-1}) of the three lines near λ 3320 ($\lambda\lambda$ 3340.74, 3312.30, and 3299.36) should be larger by a factor 12.9 (the relative A_{ij} ratio ~2.5 multplied by the factor 3320/644). Therefore, the λ 644 lines should have a total intensity of ~400 $\times$ 10^{-13} erg cm^{-2} s^{-1} and constitute an important EUV contributor to the Bowen decays. The λ 644 lines were reported in the spectrum of the Sun obtained by Behring (1976) in the study by Bhatia et al. (1982) and in the Skylab spectrum of the Sun obtained by Vernazza & Reeves (1978). Their observed intensities were found by Bhatia et al. (1982) to be in excellent agreement with those obtained in a detailed calculation of the O III EUV spectrum of the quiet Sun, when the process of photoexcitation by He II Ly-α was included.
   Moore's tables (1993) report also a transition (mult. UV 17.04) from 2p3p$^3S_1$ (297 558.66 cm^{-1}, 36.89 eV) to 2s 2p^3 $^3S^\circ_1$ (197 087.7 cm^{-1}, 24.44 eV) that corresponds to the λ 995.31 line. This transition between two S levels violates the pure LS coupling selection rules

and the line intensity should be very weak. However, it is worth reporting the presence on BEFS spectra of a medium-weak line at λ 995.3 ($I \sim 1.9 \times 10^{-13}$ erg cm^{-2} s^{-1}) that lacks any other reliable identification. It is worth noting that the Froese Fisher atomic model for O III supports intermediate coupling versus pure LS coupling. We thank the referee for pointing out the possibility that the 2p3p^{3}S$_1$ level be mixed with level 2p3p^{3}P$_1$. This interaction between states of different L is an indication of departure from pure LS coupling.

4. The three 2p3p ^{3}D$_{1,2,3}$ levels (294 223.07 cm^{-1}, 36.48 eV, 294 002.86 cm^{-1} 36.45 eV, and 293 866.49 cm^{-1} 36.43 eV) are fed by three decays from 2p3d 3P$^\circ_2$ (329 469.80 cm^{-1}, 40.85 eV) at λ 2836.28, λ 2818.66 and λ 2807.90 respectively, and produce six rather weak lines that fall between λ 3754 and λ 3810.
   The decay from 2p3p ^{3}D$_3$ (294 223.07 cm^{-1}) produces the λ 3759.87 line, the only secondary line that is a "pure" O1 line. Unfortunately the line falls in a blend with the strong and wide [Fe VII] line λ 3759. This prevents a detailed analysis. Additional decays (with slightly weaker A_{ij}) from this level are possible through the EUV lines at λ 658.58 and λ 574.06.
   The observed decays from the 2p3p ^{3}D$_2$ level (294 002.86 cm^{-1}) produce the two weak lines at λ 3754.67 and λ 3791.26. The sum of the number of photons in these two lines (=21.4 $\times$ 10^{-3} cm^{-2} s^{-1}) is close to that (=18.5 $\times$ 10^{-3} cm^{-2} s^{-1}) in the parent line λ 2818.66.
   However, from "The Atomic Line List 2.05" one can see that there are competitive decays from 2p3p ^{3}D$_2$ with similar A_{ij} in the EUV region at λ 574.8, and λ 659.5. Therefore, either the λ 3754.67 and λ 3791.26 lines are slightly blended or the 2p3p ^{3}D$_2$ level is partially populated by the charge-exchange (CE) mechanism, as reported in the following lines.
   The decays from level 2p3p ^{3}D$_1$ (36.43 eV, 293 866.49 cm^{-1}) produce the three lines at $\lambda\lambda$ 3757.21, 3774.00, and 3810.96. This level is the lower level of the λ 2807.90 line. It is worth noting that the λ 2807.90 line is barely detectable ($N_\nu = 0.4 \times$ 10^{-3} cm^{-2} s^{-1}) in the STIS near UV spectrum that has high resolution (see Fig. 7); instead, two of the subsequent decay lines, i.e. λ 3757.21 and λ 3774.40, are present both in STIS and UVES spectra (N = 9.96 $\times$ 10^{-3} cm^{-2} s^{-1}) while the third one at λ 3810.96 falls in a blend. This suggests that the 2p3p ^{3}D$_1$ level is mainly populated by charge-exchange, as reported in Aller (1984) and Dalgarno & Sternberg (1982).
5. The three 2p3s^{3}P$^\circ_{0,1,2}$ levels (267 634.00, 267 377.11, and 267 258.71 cm^{-1}, 33.18, 33.15, and 33.14 eV) are populated by 14 near UV/optical lines of the secondary decays from levels 2p3p ^{3}P$_{0,1,2}$, 2p3p ^{3}S$_1$, and 2p3p ^{3}D$_{1,2,3}$. The number of decays to these levels (with a negligible contribution from the CE process) is 516.3, 259.1 and 102.5 $\times$ 10^{-3} cm^{-2} s^{-1} respectively. The total number of decays is 878 $\times$ 10^{-3} cm^{-2} s^{-1} to be compared with the 2444.1 $\times$ 10^{-3} cm^{-2} s^{-1} primary decays from level 2p3d ^{3}P$^\circ_2$ (O1). We note that the sole permitted decays from these three 2p3s^{3}P$^\circ_{0,1,2}$ levels are through the six EUV resonance lines of mult. UV 6 near λ 374 (see also Fig. 6) that are important in the context of the Bowen secondary N III fluorescence (see Sect. 6.1).

We point out that unlike the primary lines that are "pure" O1 or O3 lines, most secondary lines are "mixed" O1 + O3 lines (see also Sects. 4.1 and 4.4). However, most O3 lines are very weak, and their contribution to the secondary decays is generally negligible. The sole exception is that of the λ 3122 line which, however, represents a contribution of about 2% to the total population of the 2p3p ^{3}S$_1$ level. This justifies the neglect of the O3 contribution to the secondary lines in most of the previous considerations.

5. The other O III lines

In principle, recombinations and charge-exchange (CE) could be effective in populating some high levels of O III and provide some contribution to the intensity of the Bowen lines.

To check for the effectiveness and the relative importance of these processes we have looked for the presence in STIS and UVES spectra of such O III lines coming from high-lying levels, whose excitation is comparable to that of the Bowen lines.

The inspection has revealed the presence of a small number of weak lines in the near-UV optical range, the strongest one being the λ 2983.81 line (mult. UV 18, u.l. = 38.01 eV, $I = 9.2 \times$ 10^{-14} erg cm^{-2} s^{-1}). The only other possible detection in the near-UV is the (weak) line at λ 2959.72 (UV 19.12, 40.26 eV) with $I = 1.44 \times 10^{-14}$ erg cm^{-2} s^{-1}). This line would feed the λ 5592.25 line (mult 5, u.l. = 36.07 eV), that is important in the context of the charge-exchange process (see below).

In the optical range, in UVES spectra, we have detected the three weak lines of mult. 8 (u.l. = 40.27 eV) at λ 3265.32 ($I = 2.54 \times 10^{-14}$ erg cm^{-2} s^{-1}), λ 3260.84 ($I =$ 1.76 $\times$ 10^{-14} erg cm^{-2} s^{-1}) and λ 3267.20 ($I = 2.10 \times$ 10^{-14} erg cm^{-2} s^{-1}), and the λ 3455.06 line of mult. 25 (u.l. = 48.95 eV) with $I = 0.96 \times 10^{-14}$ erg cm^{-2} s^{-1}). The important λ 5592.25 line of mult. 5, (u.l. = 36.07 eV) whose presence is associated with the CE process is detected only in UVES, with intensity of 1.2×10^{-14} erg cm^{-2} s^{-1}.

Therefore, the contribution by recombinations and/or CE to the observed intensity of the O III Bowen lines is generally negligible, with the exception of the six weak lines in the decay from the 2p3p^{3}D$_{1,2,3}$ term, whose individual intensities are in the range of 0.2–0.8 $\times$ 10^{-13} erg cm^{-2} s^{-1}.

6. The N III 4640 lines

6.1. The excitation mechanism

Bowen (1934, 1935) pointed out that, by another remarkable coincidence in nature, the O III resonance line λ 374.432 (one of the six decays from 2p3s ^{3}P$^\circ_{0,1,2}$ to the ground term 2p^2 ^{3}P$_{0,1,2}$ in the final decays of the Bowen lines) has nearly the same wavelength[1] as the two resonance lines of N III λ 374.434 and λ 374.442. Therefore, photoexcitation by O III 374.432 can populate both the 3d ^{2}D$_{5/2}$ level (267 244 cm^{-1}) and the 3d ^{2}D$_{3/2}$ level (267 238.40 cm^{-1}) of N III from the 2p ^{2}P$^\circ_{3/2}$ level (174 cm^{-1}) of the ground term. In the decay from these two high levels, the three lines at $\lambda\lambda$ 4640.64, 4641.85 and 4634.13 are

[1] Wavelengths for the N III and O III lines in this section and in the following are from "The Atomic Lines List 2.05" (`http://www.pa.uky.edu/~peter/newpage`), rounded to the third decimal digit. We note that these wavelengths are the same as those reported in Wiese et al. (1996), and in the NIST Web site (`http://physics.nist.gov/PhysRefData/ASD/index.html`) as Ritz wavelengths. These wavelengths come from the analysis by Pettersson 1982 and they are supposed to be correct to about 0.0005 Å at 250 Å and to 0.002 Å at 500 Å. Interpolation suggests a wavelength uncertainty of 0.00125 Å (1.0 km s^{-1}) near λ 374).

emitted, and in the subsequent decay two additional lines at λ 4097.36 and λ 4103.39 are produced. The relevant levels and transitions are reported in Fig. 13 and Table 7. Each level has also been identified by a number index from 1 to 7 in order to facilitate reading the text. See also Kastner & Bhatia (1991) (hereinafter KB91) and Kallman & McCray (1980) for further theoretical considerations and quantitative evaluations.

These optical N III lines are observed as quite strong emission lines in planetary nebulae, X-ray binaries, symbiotic stars and novae in the early nebular stages.

KB91, however, from a direct comparison of the observed line ratios with the theoretically predicted ratios expected from the postulated Bowen process of selective photoexcitation, have challenged the common interpretation that these N III emission lines originate from a secondary Bowen fluorescence. Their main argument against Bowen fluorescence is that the observed I_{4634}/I_{4640} ratio indicates a relative population ratio N_6/N_7 close to the "statistical" value 0.667 (where level 6 is 3d $^2D_{3/2}$ and level 7 is 3d $^2D_{5/2}$, see also Fig. 13). Instead, in the case of Bowen fluorescence, a much lower value (about 1/9) is expected as a consequence of the fact that $A_{2,19}/A_{2,20} \sim 0.167$ and $g_{19}/g_{20} = 4/6$. KB91 did not indicate which physical process could be responsible for the thermal population ratio that apparently existed. After tentatively suggesting recombination and charge-exchange, they ruled out both processes after specific considerations.

In a subsequent paper, Ferland (1992) suggested that the optical N III lines could be excited by direct continuum fluorescence (CF). While the Bowen mechanism would pump both the 3d $^2D_{3/2}$ and 3d $^2D_{5/2}$ levels from the excited level 2p $^2P_{3/2}$ of the ground term (with the A_{ij} and g factors favoring level 3d $^2D_{5/2}$ over level 3d $^2D_{3/2}$) continuum fluorescence would pump the level 3d $^2D_{5/2}$ from the excited level of the ground term and the 3d $^2D_{3/2}$ level predominantly from the ground level 2p $^2P_{1/2}$ of the ground term, (via the 374.198 transition) with a minor contribution (about 20%) from the excited level. As a result, (the A_{ij} of the transition from the $^2P_{1/2}$ level of the ground term being comparable to that of the transition from the $^2P_{3/2}$ level) the relative population of the 3d $^2D_{5/2}$ and 3d $^2D_{3/2}$ levels would become comparable, with the same result for the intensities of the three decay lines near λ 4640, thus reconciling the predicted intensities with the observations.

In a very recent paper, Eriksson et al. (2005) have presented a set of semi-empirical equations for the prediction of the relative intensities for the N III lines that are generated by the Bowen mechanism. They have also suggested an additional pumping channel associated with the O III λ 374.162 line (one of the six resonance lines in the final decay of the primary Bowen mechanism) that could pump the N III λ 374.198 line.

Eriksson et al. have obtained the intensities of the O III Bowen excited lines (2800–3900 Å) from IUE data of 1993 and ground-based data of the same year (Mc Kenna et al. 1997). The N III line intensities have been obtained also from Mc Kenna et al. (1997). Instead, the line widths for the O III and N III lines and the relative velocity shifts have been obtained from IUE data (SWP29535) of 1986 (see Sect. 6.4 for further comments).

In the case of RR Tel, Eriksson et al. have predicted a line ratio (relative strength) $I_{4634}/I_{4640} = 0.245$, which is too low relative to their observed values (=0.47), and have ruled out this additional line fluorescence channel as the main one responsible for populating level 6. They have concluded that the two 3d $^2D_{3/2,5/2}$ levels are predominantly populated by processes other than the Bowen mechanism and have suggested that radiative recombination could be the main population process of these

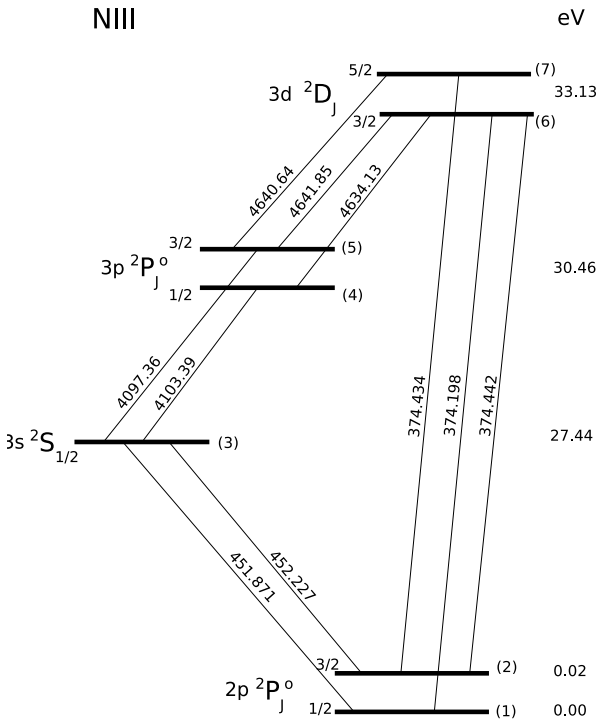

Fig. 13. A partial Grotrian diagram for N III. Levels are identified by a number index 1–7 to facilitate reading the text.

levels, although, as they pointed out, this process cannot explain some discrepancies between the predicted and observed relative intensities of the 4641.85 and 4640.64 lines.

6.2. The N III lines intensities in RR Tel

ELI and *FWHM*s for all N III subordinate lines specifically involved in the Bowen fluorescence process have been measured in STIS and FEROS spectra.

We note (see also Sect. 2.1) that the STIS data are absolutely calibrated but suffer from a limited spectral resolution in the optical range (about 8000). Instead, the FEROS data are not absolutely calibrated but have higher spectral resolution (about 60 000). Thus, STIS data provide a quite good estimate of the absolute line flux, while the FEROS data provide very accurate line ratios and good *FWHM*s measurements.

The re-calibration of FEROS (see Sect. 2.4) has also allowed us to obtain reliable ELI and reliable line ratios for a few N III emission lines that are clearly observed on FEROS but are not detected or are confused with noise in the STIS grating spectra in the optical range.

Table 7 gives the measurements for the individual lines and their average (STIS and FEROS) intensities relative to the reference line λ 4640.64. The intensity of the 4103.39 line is rather uncertain because it falls on the red wing of the strong H_γ line. The data also indicate that $I_{4640.64}/(I_{4641.85}+I_{4634.13}) = 1.59$ and $I_{4634.13}/I_{4640.64} = 0.49$, close to the value (0.47) found by Eriksson et al. (2005).

The N III lines have *FWHM* values near 33.2 km s^{-1}, a value that is close to that (35.3 km s^{-1}) found for the O III Bowen lines. The average relative displacement (O III – N III) is -1.45 km s^{-1} (Eriksson et al. instead found 4–5 km s^{-1}).

Table 7. Wavelengths, A_{ij} values, STIS and FEROS intensities (10^{-13} erg cm^{-2} s^{-1}), *FWHM* (km s^{-1}), relative intensities ($I_{4640.64}$ = 1.00), and photon number for the N III emission lines associated with the Bowen fluorescence. The continuum of FEROS has been scaled to that of STIS.

$\lambda_{\rm air}$(Å)	A_{ij}	STIS	FEROS	*FWHM*	Rel. int.	N_v
4097.36	8.66e+07	2.05	1.75	35.3	0.59	0.042
4103.39	8.62e+07	–	(0.90)	(31.0)	(0.31)	(0.022)
4634.13	6.00e+07	1.69	1.41	32.0	0.49	0.039
4640.64	7.17e+07	3.46	2.89	31.8	1.00	0.081
4641.85	1.19e+07	(0.60)	0.40	33.7	0.14	(0.014)
374.198	1.05e+10	–	–	–	–	–
374.434	1.26e+10	–	–	–	–	–
374.442	0.21e+10	–	–	–	–	–

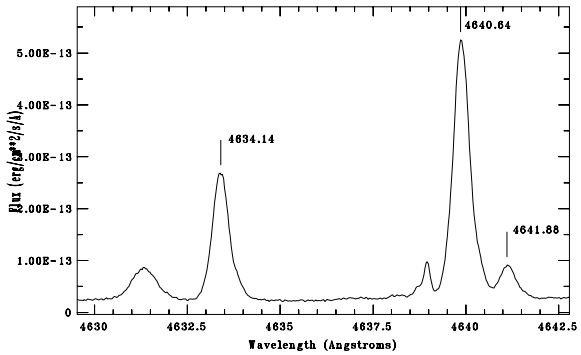

Fig. 14. The FEROS spectrum of the three N III lines close to λ 4640. The continuum has been scaled to that of STIS.

6.3. The exclusion of continuum fluorescence and radiative recombination as the excitation mechanism of the N III λ 4640 lines

As already mentioned in Sect. 6.1, in order to explain the fact that the the N III λ 4640 lines have relative intensities that are indicative of a "statistical" population of the 3d ^{2}D$_J$ levels, Ferland (1992) argued that these lines are the result of continuum fluorescence.

However, if this mechanism were effective for the three N III lines near λ 374 (mult. UV 5) one would expect a similar excitation mechanism also for the other EUV resonance lines of N III. Inspection of "The Atomic Line List 2.05" and of the Moore's (1993) tables of spectra in the range $\lambda\,\lambda$ 250–500 shows the presence of several resonance lines (multiplets) with A_{ij} values (intensities) similar to those of the 374 lines, i.e. $\lambda\lambda$ 451.87 + 452.23. (UV 4), 332.33 + 332.14 (UV 5.01), 323.49 + 323.61 + 323.67 (UV 6), 314.71 + 314.86 + 314.89 (UV 7), 311.64 + 311.55 + 311.72 (UV 7.01), 292.44 + 292.59 (UV 7.04), 282.21 + 282.07 (UV 7.06) and other multiplets of weaker intensity. For each level of the upper term of these multiplets we have selected the strongest decays (about a dozen lines between λ 1385 and λ 4205, i.e. $\lambda\lambda$ 1387.30, 1387.38, 1387.99, 1804.49, 1885.06, 1885.22, 2248.36, 2249.63, 2334.26, 2335.61, 3304.98, 3307.58, 3307.70, 4201.26, 4855.19, 4874.46, 4882.03) and checked for their presence in the STIS + UVES + FEROS spectrum of RR Tel.

The search has given a definite negative result. The absence of decays from the upper level of strong resonance lines that are likely to be pumped by continuum fluorescence is hardly compatible with the process of CF since it is hard to explain how this mechanism might work only for a selected group of lines viz. the 4640 s.

Moreover, if CF were effective, it should work also in the case of the O III resonance lines (and other resonance lines in that range) and one would expect, for example, CF to pump the three upper levels (2p3d)^{3}P$_{2,1,0}$ of the six resonance lines near λ 303. In this case, from the A_{ij} and g values (the I_{ij} values being the same for all transitions) one would expect to see a "statistical" relative population ratio 5:3:1 within these three upper levels and therefore a corresponding relative intensity ratio for the three "pure" primary lines (λ 3132.79, λ 3121.64 and λ 3115.68) that emanate from these levels (since they all have similar A_{ij} values =1.50×10^8), unlike what is observed. If, instead, one assumes that the observed intensity is a combination of contributions from Bowen fluorescence and continuum fluorescence this would imply that CF, if present, is, at best, very marginal since observations show that the (2p3d)^{3}P$_0$ level (upper level of λ 3115.68) is very weakly populated.

Concerning other physical processes such as radiative recombination as the main population process of the 3d ^{2}D$_J$ levels (see also the considerations by KB91 and Eriksson et al. 2005 in Sect. 6.1), we have checked in detail the possible presence of recombination lines of N III in the RR Tel spectrum. In particular we have searched in "The Atomic Lines List 2.05" all possible decays into the two upper levels 3d ^{2}D$_{5/2}$ (267 244 cm^{-1}) and 3d ^{2}D$_{3/2}$ (267 238.40 cm^{-1}) of the N III 4640 lines, that is for possible parents of these lines. The strongest lines, besides a sextet near λ 1324, are those of mult. UV 23 with three lines near λ 2248 and those of mult. UV 24 with two lines near λ 1885. None of these lines has been detected. Therefore the 4640 lines are not fed by decays from higher levels. We have also checked for the presence of high-lying subordinate lines with high A_{ij} and excitation level similar to that of the 4640 lines, e.g. the lines of mult. UV 22, 22.01, and 22.02., but this search has also given negative results.

An inspection of the RR Tel spectrum for the possible presence of the strongest transitions into the two lower levels 3p ^{2}P$^\circ_J$ (17 and 18) of the three 4640 lines, e.g. λ 1387.30, λ 1387.38, and λ 1804.49 (whose sum of the A_{ij} is about ten times larger than the A_{ij} of the λ 4634.13 and λ 4641.85 lines) has also given a negative result.

Therefore, recombination is ruled out by the absence of possible decays from higher levels into the three 4640 lines, and the absence of other subordinate lines with similar A_{ij} and excitation as the 4640 lines. In conclusion: neither continuum fluorescence nor radiative recombination seem effective in producing the observed N III emission lines in RR Tel. It is hard to explain how these processes may excite levels 6 and 7 of N III only, which indicates, instead, that some kind of selective process is present.

6.4. The role of multiple scatterings in the resonance lines of O III and N III

Continuum fluorescence and radiative recombination being ruled out, we must consider if and how a selective process like line fluorescence, could be responsible for the observed relative lines ratio in the N III 4640 lines.

We are supported in this investigation by the circumstantial evidence that the presence of the O III Bowen lines is generally associated with that of the N III 4640 lines in all well studied objects, a clear indication that the excitation mechanism is similar.

We recall that Eriksson et al. (2005) have taken into account the possibility of an extra pumping of level 6 (3d ^{2}D$_{3/2}$) from level 1 (which is required for approaching the observed

I_{4634}/I_{4640} line ratio) by the near coincidence between the N III λ 374.198 and the O III λ 374.162 lines. They have obtained a population ratio $N_6/N_7 = 0.29$ and a line ratio $I_{4634}/I_{4640} = 0.245$ which is too low relative to their observed values (=0.47) and concluded that this mechanism is not effective.

Eriksson et al. (2005), using the study of Pettersson (1982) have also pointed out that the combined effects of the uncertainties in the wavelengths of the ground term transitions of N III and O III near λ 374 and of the relative velocity shifts could introduce larger uncertainties for the overlap of the profiles of the pumping and of the pumped lines and therefore for the relative line strengths. However, the Pettersson paper (1982) suggests uncertainties of 0.0005 Å at 250 Å and 0.002 Å at 500 Å, which means an uncertainty of 1.0 km s^{-1}.

The velocity separation between O III λ 374.162 and N III λ 374.198 is close to 30 km s^{-1} and the effectiveness of pumping of N III level 6 from level 1 by O III λ 374.162 crucially depends on the overlap between the two lines (instead, the pumping of levels 6 and 7 of N III from level 2 are easily explained by the almost full overlap (coincidence) between the O III λ 374.432 and the N III λ 374.434 (N1) and λ 374.442 (N2) lines). The negative conclusion by Eriksson et al. (2005) derives from the (allegedly) small overlap between the profiles of the O III λ 374.162 and N III λ 374.198 lines, that could not guarantee the required pumping of level 6 from level 1.

In this context, it should be noted that Eriksson et al. have based their calculations of line overlap on the measurements of the Gaussian widths (=0.6**FWHM*) of the *intercombination* lines of N III] λ 1750 and O III] λ 1660 in IUE spectra of 1986. The same width has been assumed in the calculation of the overlap between the profiles of the *resonance* lines of O III λ 374.162 and N III λ 374.198. Instead, in STIS and FEROS spectra, the subordinate lines of O III and N III are wider than the intercombination lines by about 5 km s^{-1}, with the effect of increasing the line overlap.

However, what is of much higher relevance is the fact that both the six O III λ 374 resonance lines that connect the ground term $2p^2\ ^3P$ with the term $2p3s\ ^3P$ and the three N III resonance lines λ 374 that connect levels 1 and 2 with levels 6 and 7 are all *optically thick*, with optical depths on the order of 1000 (see appendix for an approximate estimate), while Eriksson et al. (2005) in their semi-empirical calculations have assumed that all transitions are optically thin.

We suggest here that multiple scattering in the O III λ 374.162 resonance line has the effect of increasing the pumping of level 6 from level 1 of N III, as compared to the optically thin case. Under optically thick conditions the O III resonance-line photons will suffer many scatterings ($\langle N\rangle \sim \tau_0 \cdot \sqrt{\ln(\tau_0)}$) within the nebula. The probability per single scattering that a λ 374.162 photon of O III will excite level 6 of N III (instead of level $2p3s\ ^3P_1$ of O III) depends mainly on the overlap between the O III λ 374.162 and the N III λ 374.198 lines and on the relative N III/O III ground term population (abundances- ionization fraction) ratio.

We have no direct information on the widths of the O III resonance lines. In our spectra the observed subordinate lines (most of them being the fluorescence lines) have *FWHM* close to 35.3 km s^{-1} (while the intercombination lines of O III near λ 1666 and those of N III lines near λ 1750 have smaller *FWHM*s values, close to 29.7 and 25.7 km s^{-1} respectively). Assuming Gaussian widths, the line overlap fraction is close to 0.30. However, this is almost certainly a lower limit since it is likely that the resonance lines are wider than the recombination and the intercombination lines because of line broadening by Doppler shifts. Opacity broadening ($\propto \sqrt{\ln(\tau_0)}$) will significantly affect their shape and line center optical depths close to 1000 will result in line widths 2.6 times larger than that of the optically thin case (Oegerle et al. 1983). Also, the shape of the resonance lines is better represented by a Lorentzian profile, with wider wings than the Gaussian one. Moreover as mentioned in Sect. 4.3, the profile of the O III Bowen line is aymmetric toward the red with a maximum velocity in the red wing of about 100 km s^{-1}.

In any case, with the assumptions that: 1) the overlap between the O III λ 374.162 and the N III λ 374.198 resonance lines is about 0.30 (a lower limit, as derived from the subordinate lines of the same ions), 2) the abundance ratio N III/O III is about 1/15 (the abundance ratio N/O is about 3 and the ionization fraction ratio (N III/N)/(O III/O) is about 5 in the region where the two ions co-exist, HN86), 3) all N III is in the ground term (with relative population of the $2p\ ^2P^\circ_{1/2}$ level given by its statistical weight =1/3), one obtains a rough estimate of $0.30 \cdot 0.0667 \cdot 0.333 = 6.67 \times 10^{-3}$ as the direct probability per single scattering that a λ 374.162 photon of O III will directly excite level 6 of N III from its ground level $^2P^\circ_{1/2}$ (Hydrogen photoionization is neglected: He^{+2} region: no neutral H). However, since the optical depth (or the number of scatterings before the line escapes the nebula) for the O III resonance λ 374.162 line is about 1000, (see Appendix) the probability that the level 6 of N III is *not* excited after this number of scatterings is $(1–0.0066)^{1000} \sim 0.001$. See Ferland (1992) for similar considerations in the case of resonance fluorescence.

Once the $3d\ ^2D_{3/2}$ level (level 6) of N III is pumped, it can decay either via resonant scattering with emission of the (19 → 1) λ 374.198 line (or the less likely (19 → 2) λ 374.442 line) or via emission of one of the two subordinate lines at λ 4634.13 and λ 4641.85. The A_{ij} branching ratio from the upper level (6) (see Table 7) favours resonant scattering with respect to the cascade routes via the λ 4641.85 and λ 4634.13 lines by a factor about 175 = $(1.26 \times 10^{10})/(7.19 \times 10^7)$. Therefore, the probability of conversion into the cascade route in a single act (decay) is =0.0057. However, if the number of scatterings of the N III λ 374.198 resonance line is about 1000 (see Appendix), the probability that the line will not be converted into the optical λ 4634 + λ 4641 lines after this number of scatterings is on the order $(1 - (A_{19,18} + A_{19,17})/(A_{19,1} + A_{19,2}))^{1000} \sim 0.01$.

Therefore, multiple scattering of the λ 374 resonance lines of O III and N III have the net effect of converting a significant fraction of these photons into photons of the N III subordinate lines at λ 4634 and λ 4641 that can easily escape from the nebula. We point out that while the O III λ 374 lines are pure resonance lines, without alternative decay routes from their upper levels, the N III 374 photons have an escape route through conversion to the $\lambda \sim 4640$ and $\lambda \sim 4100$ lines (and other decays). It is obvious that in the optically thin case the pumping efficiency is critically dependent on the degree of line overlap, while in the optically thick case line broadening and multiple scattering will strongly increase the pumping efficiency.

It should also be noted that high oxygen and nitrogen abundances (about 4 × solar), such as those generally found in the ejecta of novae would produce more intense O III Bowen lines as well as more intense N III λ 4640 lines because of the larger optical depths in the O III and N III resonance lines (see also Netzer et al. 1985).

Clearly, the extra contribution to the population of level 6 is added to that produced by the excitation via the O III λ 374.432 line. Note that the λ 374.162 and the λ 374.432 O III lines

Table 8. Wavelengths (Å) and A_{ij} values, for the O III resonance lines associated with the Bowen fluorescence.

λ_{vac}	A_{ij}	λ_{vac}	A_{ij}
303.413	3.86E+09	373.803	9.92E+08
303.461	1.16E+10	374.004	1.32E+09
303.517	2.89E+09	374.073	2.97E+09
303.622	2.89E+09	374.162	9.90E+08
303.695	4.81E+09	374.328	3.95E+09
303.800	8.65E+09	374.432	1.65E+09

emanate from the same upper level (see Fig. 6) and that the intensity ratio of the two lines is ∼0.600 because of the relative A_{ij} ratio (Table 8). As already mentioned in Sect. 6.1, if level 6 is excited by λ 374.442 only, the population ratio N_6/N_7 is =0.111 (because of the relative A_{ij} ratio =0.167 and statistical weights ratios =0.666) and the expected I_{4634}/I_{4640} ratio becomes ∼0.09, while the observed ratio is ∼0.49. Therefore, in order to achieve this line ratio the relative population ratio N_6/N_7 must be close to about 0.57.

Simple calculations of the photoexcitation rate of levels 6 and 7 of N III from the ground term ($\propto n_i \cdot g_j/g_i \cdot A_{i,j} \cdot I_{i,j}$), assuming LTE population for the N III ground levels, show that if all O III 374.162 photons are effective in the population of level 6 of N III, the N_6/N_7 ratio becomes ∼0.444 and, correspondingly, the I_{4634}/I_{4640} ratio becomes ∼0.37. This ratio is slightly lower than the observed one (∼0.49).

6.5. An additional pumping channel?

Without invoking deviations from LTE in the population of the two levels of the ground term of N III in order to obtain the required ratio (a physical condition that would not be too surprising, on account of the low electron density and of the fact that the radiative processes seem to dominate over the collisional ones), we suggest here that the missing contribution could arise also from the O III λ 374.073 line, one of the two decays from level 2p3s $^3P^\circ_2$. Although the line center separation is 101 km s^{-1}, even a small overlap between the line wings would ensure some degree of pumping if the line optical depth is high.

Using the same considerations adopted in the previous section for the O III λ 374.162 line (but assuming, in a conservative approach, only 5% as the overlap fraction between the N III λ 374.198 and the O III λ 374.073 line profiles) one obtains a rough estimate of $0.05 \cdot 0.0667 \cdot 0.333 = 1.1 \times 10^{-3}$ as the direct probability per single scattering that a O III λ 374.073 photon will directly excite level 6 of N III from its ground level $^2P_{1/2}$. However, since the optical depth of the O III λ 374.073 resonance line is about 6000 (larger than that of the O III λ 374.162 line), the probability that level 6 of N III is *not* excited after this number of scatterings is again very low $(1–0.0011)^{6000} \sim 0.0005$.

One should also note that the smaller overlap is compensated by the much larger line intensity of O III λ 374.073 relative to O III λ 374.162. In fact, as a result of the combined effect of the larger number of decays to the O III 3p3s $^3P^\circ_2$ level at 267 634 cm^{-1} relative to the O III 3p3s $^3P^\circ_1$ level at 267 377 cm^{-1} (516.3 and 259.1 $\times$ 10^{-3} cm^{-2} s^{-1} respectively, see Sect. 4.6) and of the line branching ratios within each of these levels, the O III λ 374.073 line is about six times stronger than the O III λ 374.162 line and about 3.6 times stronger than the O III λ 374.432 line. As an illustration, the relative intensities of the five resonance lines of O III that fall between lambda 374.004 and lambda 374.432 are reported in Fig. 15 together with their resulting profile for *FWHM* = 100 km^{-1}. From this figure one can see that, as a result of the strong contribution of the O III λ 374.073 line, the combined intensity near the N III λ 374.198 line is higher by about 30% than that corresponding to the O III λ 374.162 line alone.

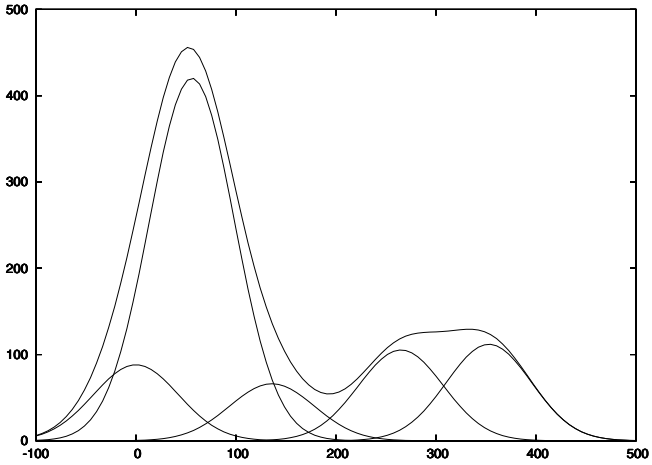

Fig. 15. The five O III resonance lines close to lambda 374, with relative height proportional to their intensity, and *FWHM* = 100 km s^{-1}. The upper line represents the sum of the five components. The *x*-axis gives the line separation in km s^{-1}, with zero-point at λ 374.00.

In this case, simple calculations of the radiative rates show that the relative flux ratio $I_{374.198}/I_{374.434}$ would be just about 20% lower than that required (in the optically thin case) to populate the N III levels 6 and 7 with the ratio required by the observations. Moreover, a red-wing excess/asymmetry in the strong O III λ 374.073 line, as observed in all O III lines, would increase the flux near λ 374.198 and produce a ratio close to that required. However, we want to explicitly point out again that it is the process of multiple scatterings (optically thick conditions) which is more effective in increasing the pumping efficiency.

As a circumstantial support of this "new" pumping channel of level 6 of N III by O III λ 374.073, despite the separation of about 100 km s^{-1} between the line centers, one notes that in the case of the well observed O III O3 fluorescence channel the line separation between He II Ly-α λ 303.782 and O III 303.893 is not much smaller (about −88.2 km^{-1}), while in the process that excites the 2p3p $^3P^\circ_0$ level of O III and produces the two weak lines observed at λ 3115.68 and λ 3408.12, the velocity separation between the He II Ly-α line and the O III λ 303.461 line is −250 km^{-1}. This latter excitation process, that is called "other" in KB96, necessarily requires wide wings in the resonance line of He II 303.782, while the observed *FWHM* of the He II recombination lines is much lower, close to 60 km^{-1}. This clearly indicates that the resonance lines are much wider than the subordinate lines.

In conclusion, the λ 374.073 resonance line of O III may also contribute to the population of level 6 of N III and thus increase the population ratio N_6/N_7 to a value close to the observed one. Obviously, similar considerations could be applied to the O III λ 374.328 resonance line, whose wavelength falls midway between N III λ 374.442 and N III λ 374.198 line and therefore would provide a similar contribution to the population of levels 6 and 7 of N III.

6.6. The absolute intensities of the N III lines and the requirement of large optical depths

In Sect. 6.4 large optical depths in the resonance lines of O III and N III have been proposed as a mechanism to explain the observed intensity *ratio* in the three N III λ 4640 lines. This assumption was justified by the estimates reported in the Appendix. An additional and convincing argument in favour of this mechanism comes from the fact that the observed *absolute* intensities of the N III λ 4640 lines necessarily require large optical depths in the exciting lines.

We recall that from STIS and UVES observations one can directly derive the number of O III photons that populate the three levels of the O III 2p3s $^3P^\circ_J$ term from which the six O III lines near λ 374 have origin. Therefore, starting from the observed number of O III photons (0.26 photons cm^{-2} s^{-1}) into level 2p3s $^3P^\circ_1$ of O III (the upper level of the O III λ 374.434 line, that can populate level 7 of N III) one can provide an upper limit for the expected number of photons in the N III λ 4640.64 line.

The branching ratio from level 2p3s $^3P^\circ_1$ of O III toward the λ 374.432 line (there are two competing decays from the same level at λ 374.162 and λ 374.004) is close to 0.42 (see Fig. 6 and Table 8) and therefore about 0.11 photons cm^{-2} s^{-1} are expected in the O III λ 374.432 line. Assuming full conversion of this line into the two N III lines at λ 374.434 and λ 374.442, from the A_{ij} ratio (close to 6.0) of these two N III transitions one obtains that the number of photons cm^{-2} s^{-1} that populate level 7 (3d $^2D_{5/2}$) of N III through the λ 374.434 line is about 0.093. Assuming that level 7 (3d $^2D_{5/2}$) of N III will decay only through the λ 4640.64 line (instead of the more competitive resonant decay) one obtains the same value (0.093) for the number of photons in the λ 4640.64 line. This corresponds to a line intensity of 3.96×10^{-13} erg cm^{-2} s^{-1}.

The observed intensity (STIS) of the λ 4640.64 line is 3.46×10^{-13} erg cm^{-2} s^{-1} (corresponding to 0.081 photons cm^{-2} s^{-1}). Therefore the observed intensity of N III λ 4640.64 is only slightly less (~87%) than that expected in the limiting case of full conversion of O III λ 374.432 into N III λ 374.434 and of N III λ 374.434 into N III λ 4640.64 (and additional decays).

As already mentioned, in the optically thin case the conversion of O III λ 374.432 into N III 374.434 by line overlap would be much smaller than 1, but above all, the A_{ij} branching ratio from level 7 of N III would favour re-emission of λ 374.434 instead of λ 4640.64, by a factor $(1.26 \times 10^{10})/(7.17 \times 10^7) = 175$ and therefore the expected emission intensity in the λ 4640.64 line would be lower by a factor close to 10^3. Similar considerations can be used for level 6 and the N III λ 4641.85 and λ 4634.13 lines.

In conclusion, very low N III intensities are expected in the optically thin regime because the A_{ij} factors strongly favour re-emission of the resonance lines relative to the decays into the subordinate lines. In fact, the whole Bowen process starting from He II Ly-α and the O III transitions near λ 303.80 up to the the N III λ 4640 lines (via the O III and N III λ 374 lines) requires high optical depths in the resonance lines. In the optically thin case the intensity of the O III Bowen lines would be also negligible, and "a fortiori" that of the N III λ 4640 lines.

These considerations strongly support our previous arguments about the large optical depths in the resonance lines. Thus, the requirement of large optical depths is not an "ad-hoc" assumption but emerges in a self-consistent picture.

We recall that the efficiency of the N III Bowen fluorescence can be defined (Eastman & MacAlpine 1985) as the fraction of the O III λ 374 resonance photons arising from level 2p3s $^3P^\circ_1$ which undergoes fluorescence with N III and is converted to the N III Bowen lines near λ 4640. In the case of RR Tel, a direct counting of the photons gives a fraction 0.134/0.259 ~ 0.52. We note, however, that unlike the case of O III fluorescence in which the pumping line is unambiguously He II Ly-α λ 303.782, in the case of N III the candidate pumping lines can be as high as six (depending on the line width). Therefore the efficiency can vary from 15.3%, if one considers all the photons of the six O III lines near λ 374, to 87.0%, if one considers only the photons from the O III λ 374.432 line. Eastman & MacAlpine (1985) have provided a direct expression for the N III Bowen efficiency, based on the observed intensities of the O III and N III lines

$$y_{\rm N\,III} \sim 8.7 \; \frac{I(\rm N\,III\;\lambda\lambda\;4634, 4641, 4642)}{I(\rm O\,III\;\lambda\;3133)}.$$

In the case of RR Tel we obtain $y_{\rm N\,III} \sim 48\%$, in good agreement with the estimate from the photon fractions.

As a final remark to this section, we point out the analogy in the He II – O III fluorescence and in the O III – N III fluorescence: in the former case the pumping line is the optically thick He II Ly-α line while the pumped lines are the optically thick resonance lines of O III at λ 303.800 (O1) and λ 303.695 (O3), that are converted into longer wavelength subordinate lines, i.e. the primary and secondary Bowen decays that easily escape from the nebula (the tertiary decay is into the six resonance lines near λ 374). In the O III – N III fluorescence the pumping lines are the optically thick O III lines near λ 374 while the pumped lines are the three optically thick lines of N III near λ 374 that are converted into the subordinate λ 4640 primary lines and the λ 4100 secondary lines, that also easily escape from the nebula.

6.7. A detailed examination of the energy balance in the N III levels

1. Levels 7 (3d $^2D_{5/2}$, 267 244.0 cm^{-1}) and 6 (3d $^2D_{3/2}$, 267 238.40 cm^{-1}):
   these are the upper levels of the N III λ 4640.64 and λ 4634.13 + λ 4641.85 lines respectively. We have searched in "The Atomic Line List v.2.05" for all the strongest decays into these levels from all higher levels and checked for the possible presence of these lines in the spectrum of RR Tel. This search has given a definite negative result, primarily for the absence of the two very strong lines of mult. UV 24 λ 1885.06 and λ 1885.22 and of other strong lines. Therefore, there are no contributions to these levels other than that of the λ 374 lines. This result is in agreement with the negative result described in Sect. 6.3 concerning the absence of recombination lines. We note that the observed $I_{4634.13}/I_{4641.85}$ ratio is 3.50, while it should be close to 5.0 irrespective of any process, because the lines share the same upper level and have relative A_{ij} values =5.0. A possible explanation is that the λ 4641.85 line is partially blended. Its slightly larger *FWHM* (Table 7) supports this suggestion.
2. level 5 (3p $^2P^\circ_{3/2}$, 245 701.30 cm^{-1}):
   An examination in "The Atomic Line List 2.05" of all possible decays into level 5 (3p $^2P^\circ_{3/2}$ (245 701.30 cm^{-1}), shows that besides the λ 4640.64 and λ 4641.85 lines also other transitions are listed (e.g., λ 1387.38 and λ 1805.66) with much stronger A_{ij} values. However, these lines are not present in the RR Tel spectrum confirming that level 5 (3p $^2P^\circ_{3/2}$) is populated by the λ 4640.64 and λ 4641.85 lines only, thus supporting the fluorescence mechanism.

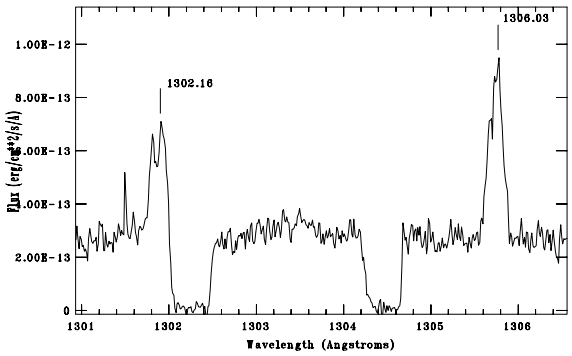

Fig. 16. The resonance O I lines close to λ 1304. The two absorption features are IS and due to the zero-volt lines of O I λ 1302.16 and Si II λ 1304.37. This latter line has fully absorbed the O I λ 1304.86 line.

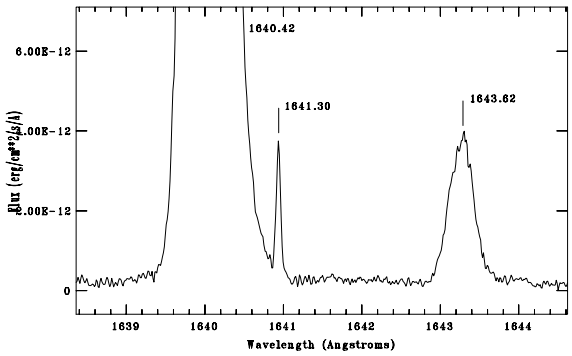

Fig. 17. The O I] λ 1641.30 intercombination line of mult. 146 UV ($3s\ ^3S^\circ_1 \rightarrow 2p^4\ ^1D_2$) on the red wing of the strong He II Ba-α λ 1640.40 line. The line at λ_{obs} = 1643.25 is O V λ 1643.62. The λ 1641.30 line shares its upper level with the three O I resonance lines close to λ 1304.

The λ 4640.64 line and the λ 4641.85 line are parents of the λ 4097.36 line. From the observed intensities one can see that the sum of the number of photons in these two lines is larger by a factor about 2.2 than the number of photons in the λ 4097.36 line. Inspection of "The Atomic Line List 2.05" shows that competing decays from the $3p\ ^2P^\circ_{3/2}$ level are two EUV transitions at λ (vac.) 691.19 and λ 871.86. The sum of the A_{ij} in these two lines is about 1.4 times larger than the A_{ij} of the λ 4097.36 line. Therefore, the difference in the number of decays is almost reconciled.

3. level 4 ($3p\ ^2P^\circ_{1/2}$, 245 665.40 cm^{-1}):
   This level is fed by the λ 4634.13 line and is the upper level of the λ 4103.39 line. The emission intensity of this line is not accurately determined because it falls in the red wing of the strong H_δ line.
   From an examination in "The Atomic Line List 2.05" of all possible decays into level 4 ($3p\ ^2P^\circ_{1/2}$ (245 665.40 cm^{-1}), one notes that also other transitions are present (e.g., λ 1387.30 and λ 1804.49) with much stronger A_{ij} values than those of the λ 4640.64 and λ 4641.85 lines. However, these lines are not present in the RR Tel spectrum confirming that level 4 is populated by λ 4634.13 only.
   From level 4 there are two competing decays at λ 691.40 and λ 872.13 and the sum of the A_{ij} of these two lines ($\sim 1.37 \times 10^8$) is about 1.6 times larger than the A_{ij} ($\sim 8.62 \times 10^7$) of the λ 4103 line. The ratio of the number of photons in the λ 4634.13 and λ 4103.39 lines (as obtained from Table 7) is about 1.8 in fair agreement with the expectations, if one takes into account the uncertainty in the emission intensity of the λ 4634.13 line.

6.8. The large optical depths in the O I resonance lines

An additional argument in support of large optical thickness in the resonance lines comes from the intensities of the three O I resonance lines of mult. UV 2 near λ 1304 ($2p^3\ 3s\ ^3S^\circ_1 \rightarrow 2p^4\ ^3P_{0,1,2}$) relative to the intercombination line at λ 1641.30 line ($3s\ ^3S^\circ_1 \rightarrow 2p^4\ ^1D_2$, mult. UV 146) with whom they share the same upper level $3s\ ^3S^\circ_1$ (76 794.98 cm^{-1}). We note that there is also the λ 2325.45 intercombination line ($3s\ ^3S^\circ_1 \rightarrow 2p^4\ ^1S_0$) that decays from the same level but its wavelength is nearly coincident with that of the CII line λ 2325.40.

The emission intensity of λ 1302.17 (l.l. = 0.00 eV) is affected by partial absorption by its IS counterpart, while the O I λ 1304.86 line (l.l. = 158.26 cm^{-1}) is fully absorbed by the Si II(3) λ 1304.37 line (l.l. = 0.00 eV). Instead, the λ 1306.03 line (l.l. 226.98 cm^{-1}) is free from IS absorption (see Fig. 16). The A_{ij} ratio 1306.03/1641.30 would favour the λ 1306.03 resonance line with respect to λ 1641.30 by a factor $0.65 \times 10^8/1.83 \times 10^3 \sim 3.5 \times 10^4$. Instead, the observed intensites on STIS are similar (1.25×10^{-13} erg cm^{-2} s^{-1} and 2.24×10^{-13} erg cm^{-2} s^{-1} respectively). Evidently, whatever is the mechanism for population of the $3s\ ^3S^\circ_1$ level (likely a decay from $3d\ ^3D^\circ$, after Ly-β λ 1025 fluorescence, through λ 11287 and λ 8446, since this latter line is present in FEROS spectra) the O I resonant photons will scatter many times and there is a very small but finite chance that at each resonant scattering decay from the upper level $3s\ ^3S^\circ_1$ will occur through the intercombination lines at λ 1641.30 and λ 2325.45.

Thus, if the scattering number is very high, processes with a small probability per scattering of destroying resonance lines can become important (Osterbrock 1962). Unlike the λ 1304 photons that are trapped resonant radiation, the λ 1641.30 photons, will leave the nebula undisturbed because of their very low A_{ij} value. Thus, the large optical depth of the λ 1304 lines has the effect of converting these resonantly trapped photons into photons of the λ 1641.30 line.

The importance of this kind of process involving the O I λ 1641.30 line for the determination of the opacity in the resonance lines has been pointed out by Jordan (1967) and by Jordan & Judge (1984) for the chromospheres of cool stars. Bhatia & Kastner (1995) have further developed this method and derived an explicit graph of the I_{1641}/I_{1302} ratio as function of $\log \tau_{1302}$. In the specific case of RR Tel they have used the measurements in IUE spectra by Penston et al. (1983) and derived $\log \tau_{1302} \sim 6.0$. This estimate should actually be considered as an upper limit because the IS absorption of the O I λ 1302 line was not taken into account. However, using our reliable I_{1641}/I_{1306} ratio from the STIS data, and "mutatis mutandis" (the A_{ij} ratio of λ 1302.16 relative to λ 1306.03 line is near 5.0) we have obtained again that $\log \tau_{1306} \sim 6.0$.

We also note that the resonance line λ 1306.03 is much wider ($FWHM \sim 43$ km s^{-1}) than the intercombination O I] line λ 1641.30 ($FWHM \sim 12$ km s^{-1}) although both lines arise from the same upper level (see also Figs. 16 and 17). This supports our previous considerations about the much larger width of the resonance lines as compared to the subordinate and intercombination ones.

7. Conclusions

By combining STIS and UVES data we have obtained very accurate measurements of the absolute intensities for about 25 He II Fowler lines and for almost all O III lines produced by the Bowen mechanism.

A new measure of reddening ($E_{(B-V)} \sim 0.00$) has been obtained from the decrement of the He II Fowler series down to the region of the series limit near λ 2060. This new $E_{(B-V)}$ value, which is in contrast with the commonly assumed value $E_{(B-V)} \sim 0.10$, has been confirmed by the observed STIS UV + optical continuum distribution, by a re-analysis of the IUE low resolution data, and by the value of the neutral H column density, obtained from the damped profile of the IS Ly-α line.

The high quality of the spectral data has allowed us to obtain the most complete set of measurements of the Bowen fluorescence lines so far reported for any astronomical source, and includes six "pure" O1 lines, seven "pure" O3 lines and the two very weak lines at λ 3115.68 and λ 3408.12 both associated with pumping in the λ 303.46 channel. This is also the first measurements of absolute intensity, for the two lines at λ 3115.68 and λ 3408.12, both associated with pumping in the λ 303.46 channel, and the first detection of two weak lines belonging to the primary decay of the O1 process, that have been found near λ 2180.

The data have also allowed a detailed study of the decays from all levels involved in the Bowen mechanism and a detailed comparison with the predictions of the theoretical models of Froese Fischer (1994) and Kastner & Bhatia (1996). In general, the observed O III emission intensities, are in very good agreement with the predictions of the Froese Fischer (1994) model. The STIS and UVES data indicate an efficiency in the O1 and O3 channels of about 20% and 0.7%, respectively. In the past (1978–1995) the O1 and O3 efficiency (obtained from a study of IUE high resolution spectra) was about 2.1 times and 4.0 times higher, respectively

A detailed study of the N III λ 4640 emission lines and of their possible excitation mechanism has shown that, recombination and continuum fluorescence being ruled out, line fluorescence remains the only viable excitation mechanism. We have pointed out the important role of multiple scattering in the resonance lines and shown that the observed relative ratios *and* absolute intensities of the N III lines can be explained in terms of line fluorescence by the three resonance lines of O III at $\lambda\lambda$ 374.432, 374.162 and 374.073 under optically thick conditions.

Appendix A: The optical depths in the O III and N III resonance lines

The line absorption cross section per atom at the line center is $\sigma_o = 8.30 \times 10^{-13}\ f_{12}\ \lambda_o^2\ (\Delta\lambda_D)^{-1}$, where $\Delta\lambda_D$ is the line *FWHM*. The optical depth at the line center is $\tau_0 = \sigma_o\ R_{neb}\ N_x$, where N_x is the number density of absorbers.

The radius of the O III emitting region (O^{+2}) nearly coincides with that of He^+ since O^{+2} has an ionization potential 54.9 eV, nearly the same (54.4 eV) as He^+ (Osterbrock & Ferland 2006). Ionization models (ibidem) also show that for an effective temperature of the exciting star greater than 40 000 K (HN86 give 200 000 K for RR Tel) the He^+ zone coincides with the H^+ zone. Therefore, the relevant radius can be obtained from the observed emission intensity in the H_β 4861 line, if N_e and the distance are known:

$$L_{4861} = h\nu_{4,2}\ \alpha_{4861}\ N_e\ N_{H^+}\ 4/3\ \pi\ R^3_{neb} = 4\pi d^2\ F_{4861}.$$

After substitution of the numeric values ($h\nu_{4,2}\ \alpha_{4861} = 1.03 \times 10^{-25}$, $N_{H^+} = 0.8N_e$, $4\pi d^2 = 1.445 \times 10^{45}$, $F_{4861} = 162.0 \times 10^{-13}$) one obtains that $R^3 = 5.40 \times 10^{58}/N_e^2$.

As an average of various N_e diagnostics for N III and O III we have obtained $N_e \sim 6 \times 10^6$, in agreement with previous estimates by HN86, and in fair agreement with the value ($Ne = 1.9 \times 10^7$) very recently obtained by Young et al. (2005) from a diagnostic based on the ratio of Fe VII lines. Therefore, in the case of a spherically symmetric, homogeneous nebula (filling factor = 1) the radius of the H^+ region is $R_{H^+} \sim 1.2 \times 10^{15}$ cm. HN86 instead obtained a value of 1.0×10^{15} cm for the whole nebula.

For the O III λ 374.432 line one has $f_{12} = 2.08 \times 10^{-2}$, and for its $\Delta\lambda_D$ we assume 0.045×10^{-8} cm (a rather conservative value that corresponds to a *FWHM* of 36 km s^{-1}, the average value from the subordinate O III Bowen lines). Assuming that: 1) $N_e = 6 \times 10^6$, 2) $N_e \sim 1.2N_H$, O/H $\sim 9 \times 10^{-4}$ (nearly solar, see Nussbaumer et al. 1988), 3) the dominant ionization stage of oxygen in a large fraction of the nebular volume is O^{+2} ($O \sim O^{+2}$) (HN86), and 4) the $2p^2\ ^3P_2$ level of the ground term of O III is thermally populated, one obtains that the optical depth in the line center of the O III 374.432 line is $\tau_0(374.432) \sim 1790$. Similar calculations for O III374.162 ($f_{12} = 2.08 \times 10^{-2}$) and O III 374.073 ($f_{12} = 6.32 \times 10^{-2}$) give $\tau_0(374.162) \sim 1075$ and $\tau_0(374.073) \sim 5370$, respectively.

The average number of scatterings $\langle N \rangle$ in the nebula is closely related to the line optical depth. For a rough estimate, we adopt the common relation ($\langle N \rangle \sim \tau_0 \cdot \sqrt{\ln(\tau_0)}$) that for the O III lines gives $\langle N_{374.432} \rangle \sim 4900$, $\langle N_{374.162} \rangle \sim 2840$, and $\langle N_{374.073} \rangle \sim 15\,700$.

For the N III 374 lines, "mutatis mutandis", i.e. 1) N/H $\sim 3 \times 10^{-4}$, 2) $N^{+2} \sim 0.2$ N since most nitrogen is in the N^{+3} ionization stage (HN86), and 3) adopting the specific f_{12} values and populations of the ground term, one obtains $\tau_0(374.442) \sim 550$, $\tau_0(374.434) \sim 1130$, $\tau_0(374.198) \sim 622$, and correspondingly that $\langle N_{374.442} \rangle \sim 1380$, $\langle N_{374.434} \rangle \sim 3000$, and $\langle N_{374.198} \rangle \sim 1580$.

References

Aller, L. H. 1984, Physics of Thermal Gaseous Nebulae, ed. L. H. Aller, Astrophysics & Space Science Library, Vol. 112
Behring, W. E., Cohen, L., Doschek, G. A., & Feldman, U. 1976, ApJ, 203, 521
Bhatia, A. K., & Kastner, S. O. 1993, Atom. Data Nucl. Data Tables, 54, 133 (BK)
Bhatia, A. K., & Kastner, S. O. 1995, ApJS, 96, 325
Bhatia, A. K., Kastner, S. O., & Behring, W. E. 1982, ApJ, 257, 887
Bessell, M. S. 1999, PASP, 111, 1426
Bowen, I. S. 1934, PASP, 46, 14
Bowen, I. S. 1935, ApJ, 81, 1
Contini, M., & Formiggini, L. 1999, ApJ, 517, 925
Crawford, F. L., McKenna, F. C., Keenan, F. P., et al. 1999, A&AS, 139, 135
della Valle, M., & Livio, M. 1995, ApJ, 452, 704
Dickey, J. M., & Lockman, F. J. 1990, ARA&A, 28, 215
Diplas, A., & Savage, B. D. 1994, ApJ, 427, 274
Downes, R. A., & Duerbeck, H. W. 2000, AJ, 120, 2007
Eastman, R. G., & MacAlpine, G. M. 1985, ApJ, 299, 785
Eriksson, M., Johansson, S., Wahlgren, G. M., et al. 2005, A&A, 434, 397
Espey, B., Keenan, F. P., McKenna, F. C., Feibelman, W. A., & Aggarwal, K. M. 1996, ApJ, 465, 965
Evans, D. S. 1967, Determination of Radial Velocities and their Applications, IAU Symp., 30, 57
Feast, M. W., Robertson, B. S. C., & Catchpole, R. M. 1977, MNRAS, 179, 499
Feast, M. W., Whitelock, P. A., Catchpole, R. M., Roberts, G., & Carter, B. S. 1983, MNRAS, 202, 951
Dalgarno, A., & Sternberg, A. 1982, MNRAS, 200, 77P
Ferland, G. J. 1992, ApJ, 389, L63
Friedjung, M. 1974, Ap&SS, 29, L5
Froese Fischer, C. 1994, Phys. Scr., 49, 323 (FF)
Galavis, M. E., Mendoza, C., & Zeippen, C. J. 1997, A&AS, 123, 159
Glass, I. S., & Webster, B. L. 1973, MNRAS, 165, 77
González-Riestra, R., Cassatella, A., & Wamsteker, W. 2001, A&A, 373, 730

Harrington, J. P. 1972, ApJ, 176, 127
Hayes, M. A., & Nussbaumer, H. 1986, A&A, 161, 287 (HN86)
Heck, A., & Manfroid, J. 1985, A&A, 142, 341
Henize, K. G., & McLaughlin, D. B. 1951, ApJ, 114, 163
Høg, E., Bässgen, G., Bastian, U., et al. 1997, A&A, 323, L57
Høg, E., Fabricius, C., Makarov, V. V., et al. 2000a, A&A, 355, L27
Høg, E., Fabricius, C., Makarov, V. V., et al. 2000b, A&A, 363, 385
Johnson, D. R. H., & Soderblom, D. R. 1987, AJ, 93, 864
Jordan, C. 1967, Sol. Phys., 2, 441
Jordan, C., & Judge, P. 1984, Phys. Scr., 8, 43
Jordan, S., Murset, U., & Werner, K. 1994, A&A, 283, 475
Kaler, J. B. 1967, ApJ, 149, 383
Kallman, T., & McCray, R. 1980, ApJ, 242, 615
Kastner, S. O., & Bhatia, A. K. 1991, ApJ, 381, L59
Kastner, S. O., & Bhatia, A. K. 1996, MNRAS, 279, 1137 (KB96)
Kaufer, A., Stahl, O., Tubbesing, S., et al. 1999, The Messenger, 95, 8
Keenan, F. P., et al. 2002, MNRAS, 337, 901
Likkel, L., & Aller, L. H. 1986, ApJ, 301, 825
Livio, M. 1992, ApJ, 393, 516
Liu, X.-W., & Danziger, J. 1993, MNRAS, 261, 465
McKenna, F. C., Keenan, F. P., Hambly, N. C., et al. 1997, ApJS, 109, 225
Mayall, M. W. 1949, Harv. Coll. Obs. Bull., 919, 15
Moore, C. E. 1993, Tables of Spectra of Hydrogen, etc. ed. J. W. Gallagher (Boca Raton, Florida: CRC Press, Inc.)
Murset, U., & Nussbaumer, H. 1994, A&A, 282, 586
Netzer, H., Elitzur, M., & Ferland, G. J. 1985, ApJ, 299, 752
Nussbaumer, H., Schmid, H. M., Vogel, M., & Schild, H. 1988, A&A, 198, 179
Oegerle, W. R., Peters, G. J., & Polidan, R. S. 1983 PASP, 95, 147
Osterbrock, D. E. 1962, ApJ, 135, 195
Osterbrock, D. E., & Ferland, G. J. 2006, Astrophysics of gaseous nebulae and active galactic nuclei, 2nd., ed. D. E. Osterbrock, & G. J. Ferland (Sausalito, CA: University Science Books)
Penston, M. V., et al. 1983, MNRAS, 202, 833
Pereira, C. B., de Araujo, F. X., & Landaberry, S. J. C. 1999, MNRAS, 309, 1074
Petterson, S. G. 1982, Phys. Scr., 26, 296
Rodríguez-Pascual, P. M., González-Riestra, R., Schartel, N., & Wamsteker, W. 1999, A&AS, 139, 183
Saraph, H. E., & Seaton, M. J. 1980, MNRAS, 193, 617 (SS)
Schachter, J., Filippenko, A. V., & Kahn, S. M. 1990, ApJ, 362, 74
Schachter, J., Filippenko, A. V., Kahn, S. M., & Paerels, F. B. S. 1991, ApJ, 373, 633
Schild, H., & Schmid, H. M. 1997, Physical Processes in Symbiotic Binaries and Related Systems, 169
Schlegel, D. J., Finkbeiner, D. P., & Davis, M. 1998, ApJ, 500, 525
Selvelli, P. L., & Bonifacio, P. 2000, A&A, 364, L1
Selvelli, P., & Bonifacio, P. 2001, Eta Carinae and Other Mysterious Stars: The Hidden Opportunities of Emission Spectroscopy, ASP Conf. Ser., 242, 367
Stone, R. P. S., & Baldwin, J. A. 1983, MNRAS, 204, 347
Storey, P. J., & Hummer, D. G. 1995, MNRAS, 272, 41
Thackeray, A. D. 1977, MmRAS, 83, 1
Vernazza, J. E., & Reeves, E. M. 1978, ApJS, 37, 485
Walker, A. R. 1977, MNRAS, 178, 245
Wallerstein, G., Garnavich, P. M., Schachter, J., & Oke, J. B. 1991, PASP, 103, 185
Whitelock, P. A. 1988, IAU Coll. 103, The Symbiotic Phenomenon, ASSL, 145, 47
Wiese, W. L., Fuhr, J. R., & Deters, T. M. 1996, Atomic transition probabilities of carbon, nitrogen, and oxygen, ed. W. L. Wiese, J. R. Fuhr, & T. M. Deters, Washington, DC: American Chemical Society ... for the National Institute of Standards and Technology (NIST) QC 453 .W53
Young, P. R., Berrington, K. A., & Lobel, A. 2005, A&A, 432, 665
Zuccolo, R., Selvelli, P., & Hack, M. 1997, A&AS, 124, 425